

INTERLIBRARY INSTRUCTIONS

BINDING INSTRUCTIONS

Call No.

E9791 1990 304	Author: Duncan, J. Title: COLOR: M. S.	Dept. RUSH _____ PERMABIND _____ PAMPHLET _____ GIFT _____ POCKET FOR MAP _____ COVERS _____ Front _____ Both _____ REFERENCE _____ Other _____
Special Instructions - Bindery or Repair <u>TUBE</u> 4/12/91		

THE GEOLOGY AND MINERALIZATION OF
THE NORTHERN PLOMOSA DISTRICT
LA PAZ COUNTY, ARIZONA

by

John Towner Duncan


A Thesis Submitted to the Faculty of the
DEPARTMENT OF GEOSCIENCES
In Partial Fulfillment of the Requirements
for the Degree of
MASTER OF SCIENCE
In the Graduate College
THE UNIVERSITY OF ARIZONA

1990

STATEMENT BY AUTHOR

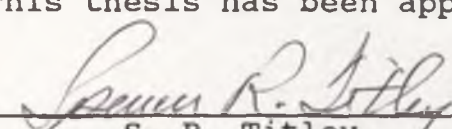
This thesis has been submitted in partial fulfillment of the requirements for an advanced degree at The University of Arizona and is deposited in the University Library to be made available to borrowers under the rules of the library.

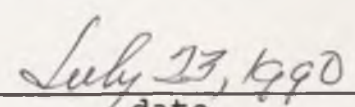
Brief quotations from this thesis are allowable without special permission, provided that accurate acknowledgment of source is made. Requests for permission for extended quotation or reproduction of this manuscript in whole or in part may be granted by the head of the major department or the Dean of the Graduate College when in his or her judgement the proposed use of the material is in the interests of scholarship. In all other instances, however, permission must be obtained from the author.

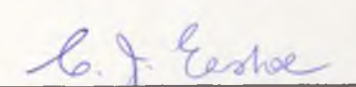
SIGNED: 

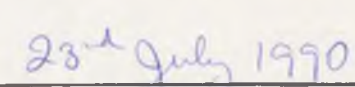
APPROVAL BY THESIS DIRECTORS

This thesis has been approved on the date shown below:


S. R. Titley
Professor of Geosciences


date


C. J. Eastoe
Geosciences Staff Scientist


date

ACKNOWLEDGMENTS

I wish to thank the members of my thesis committee. Professors Spencer R. Titley and John M. Guilbert lent their wisdom and careful review to this effort. Dr. Jon E. Spencer of the Arizona Geological Survey suggested the project and provided support for it in the form of Research Assistantships. His expertise on the regional geology of Western Arizona and detachment-fault-related mineralization were freely shared and have contributed greatly to this effort. Dr. Christopher J. Eastoe deserves special thanks for seeing this project through to completion. His guidance began in my first semester at the University of Arizona, and never flagged. He has given countless hours to this project; in the laboratory, the field, and in consultation with me. Without Dr. Eastoe's enthusiastic interest and gentle prodding this work might not have been completed in such a timely manner.

Dr. Eastoe also took the initiative in securing financial support for this study. Through his efforts, the Homestake Mining Company was persuaded to provide a generous grant to cover the costs of the project. Its support is greatly appreciated.

Thanks also go to my parents, who have been supportive in every way, throughout my extended career as a student.

Finally, my most enthusiastic thanks must go to my wife, Kathy, who married this project along with me. She has done much of the typing and drafting, and her endless patience and good spirits have made its completion a joy.

TABLE OF CONTENTS

LIST OF ILLUSTRATIONS	6
LIST OF TABLES	8
ABSTRACT	9
CHAPTER 1- Introduction	10
Location	10
Topography	10
Climate and Vegetation	12
History	13
Purpose of Study	15
Methods	16
CHAPTER 2- Geology	18
Regional Geology	18
Northern Plomosa District Geology	22
Structural Basement	22
Plomosa Detachment Fault	22
Upper Plate Rocks	24
Proterozoic Crystalline Rocks	24
Paleozoic and Mesozoic Rocks	29
Tertiary Stratigraphy	34
Bouse Arkose	36
Limestone-tuff Unit	37
Volcanic Unit	39
Plomosa Conglomerate	41
Quaternary/Recent	44
Structure	44
CHAPTER 3- Chemistry of Fine-grained Igneous Rocks	48
Primary Chemistry and K-metasomatism	48
Gains and Losses	52
CHAPTER 4- Mineralization and Alteration	58
Alteration and Replacement	58
Chlorite Stage	58
Specular hematite Replacements	64
Open-space Filling Mineralization	64
Early Quartz-Hematite Stage	64
Barite, Fluorite, Silica and Oxidized Copper	66

Table of Contents- continued

Latest, Supergene, and Unknown Stages	66
Economic Mineralization	68
Host-rock Associations	69
Structural controls on Mineralization	71
CHAPTER 5- Fluid Inclusions	74
Primary Fluid Inclusions	75
Amethyst	75
White Quartz	79
Fluorite	82
Late Fine-grained Quartz	83
Secondary Fluid Inclusions	84
Interpretation of Fluid Inclusion Data	85
CHAPTER 6- Exploration Geochemistry	96
Ratio Analysis	100
CHAPTER 7- Stable Isotope Geochemistry	106
Sulfates	108
Carbonates	117
CHAPTER 8- Discussion and Conclusions	120
REFERENCES CITED	129

LIST OF ILLUSTRATIONS

Figure	Page
1. Location of study area	11
2. Generalized cross section of a detachment fault after Spencer and Reynolds (1989b)	20
3. Photograph- Plomosa detachment fault outcrop	23
4. Photograph- Ramp of lower plate metamorphic rocks	25
5. Photograph- Folded carbonate sliver (bed?) in tectonized Proterozoic crystalline rock	28
6. Photograph- Round Mountain thrust block	30
7. Structure section- Paleozoic thrust block on Round Mountain	31
8. Stratigraphic column of the Tertiary rocks of the Northern Plomosa district	35
9. Photograph- Tertiary limestone-tuff unit	38
10. Photograph- Plomosa conglomerate on Beehive Hill	42
11. Discrimination diagram for altered volcanic rocks. After Winchester and Floyd (1977)	51
12. Isocon diagram comparing unaltered and K- metasomatized mafic volcanic rocks	54
13. Isocon diagram comparing two K-metasomatized intermediate volcanic rocks: unmineralized and mineralized	56
14. Paragenetic diagrams for 10 localities in the Northern Plomosa district	59
15. Generalized paragenetic diagram for the Northern Plomosa district mineralization	61
16. Photomicrograph- Bladed hematite and chlorite alteration assemblage in textural equilibrium	63

list of illustrations- continued

17.	Rose diagram of strikes of 29 mineralized structures in the Northern Plomosa district . . .	72
18.	Histogram of homogenization temperatures (Th) for all fluid inclusions studied	76
19.	Histogram of melting temperatures (Tm(ice)) for all fluid inclusions studied.	77
20.	Photomicrograph- Growth zone in white quartz containing fluid inclusions, from the Scotchman vein (PMD-28)	80
21.	Photomicrograph- Growth lineated primary fluid inclusions in white quartz from the Scotchman vein (PMD-28)	81
22.	Plot of Th versus Tm(ice) for primary fluid inclusions in Northern Plomosa district mineralization	86
23.	Th versus salinity plot for ore deposit classes with Northern Plomosa district added. After Wilkins et al., (1986)	92
24.	Formula and adjustment factors used to calculate "ratio values" in Table 5	102
25.	Histogram of $\delta^{34}\text{S}$ values of Northern Plomosa district barites	109
26.	Plot of $\delta^{18}\text{O}$ versus $\delta^{34}\text{S}$ for Northern Plomosa district barites and other sulfates	111
27.	Plot of $\delta^{18}\text{O}$ versus $\delta^{13}\text{C}$ for Northern Plomosa district carbonates	118
28.	Structural cross section of western Arizona including the Northern Plomosa district	122

PLATES (in pocket)

1. Geologic Map of the Northern Plomosa District
2. Sample Locations, Geochemistry and Mineralization

LIST OF TABLES

Table 1 - Whole rock and trace element analyses of fine-grained igneous rocks in the Northern Plomosa district	49
Table 2 - Sources of fluid inclusion data	88
Table 3 - Exploration geochemistry: raw analyses	97
Table 4 - Correlation coefficients between 8 ore and indicator metals in the Northern Plomosa district	99
Table 5 - "Ratio values" for 23 samples of hydrothermal mineralization in the Northern Plomosa district	103
table 6 - All stable isotope data	107

ABSTRACT

The Northern Plomosa district in west-central Arizona is a mid-Miocene Au-Cu district hosted by Miocene lacustrine sedimentary and volcanic rocks and their Proterozoic crystalline depositional basement. The host rocks are in the upper plate of the Plomosa detachment fault and are broken and tilted to the southwest by numerous northwest-striking normal faults that are the main controls on mineralization.

The primary ore minerals are native gold, chrysocolla, and malachite. Gangue minerals include specular and earthy hematite, quartz, barite, fluorite, calcite, and manganese oxides. Although open-space filling textures are locally abundant, most of the economic mineralization occurs as fault-controlled replacements in calcareous sediments.

Fluid inclusions indicate that the mineralizing system involved low temperature (150 to 250°C), high salinity (17 to 26 eq. wt. % NaCl) fluids. Oxygen, sulfur, and carbon isotopes from the hydrothermal minerals are consistently heavy and, combined with fluid salinities, suggest that the mineralizing fluids were basin brines.

CHAPTER 1

Introduction

Location

The Northern Plomosa mineral district lies within the northern half of the Linskey Northeast 7½ minute quadrangle (unpublished United States Geological Survey preliminary topographic map), at the north end of the Northern Plomosa Mountain Range in La Paz County, Arizona. The district is approximately 45 kilometers southeast of Parker, Arizona, and immediately (5km) west of the small community of Bouse (Figure 1). Excellent access to the area is provided by numerous prospect roads and jeep trails that can be entered either from Arizona Highway 72, which passes immediately to the north of the mining district, or from the gravel road leading southwest from Bouse towards Quartzsite.

Topography

The Northern Plomosa Mountains are within the Sonoran Desert region of the Basin and Range Province of the Western United States and are a relatively small, north-trending range largely surrounded by broad alluvial plains made up of thick

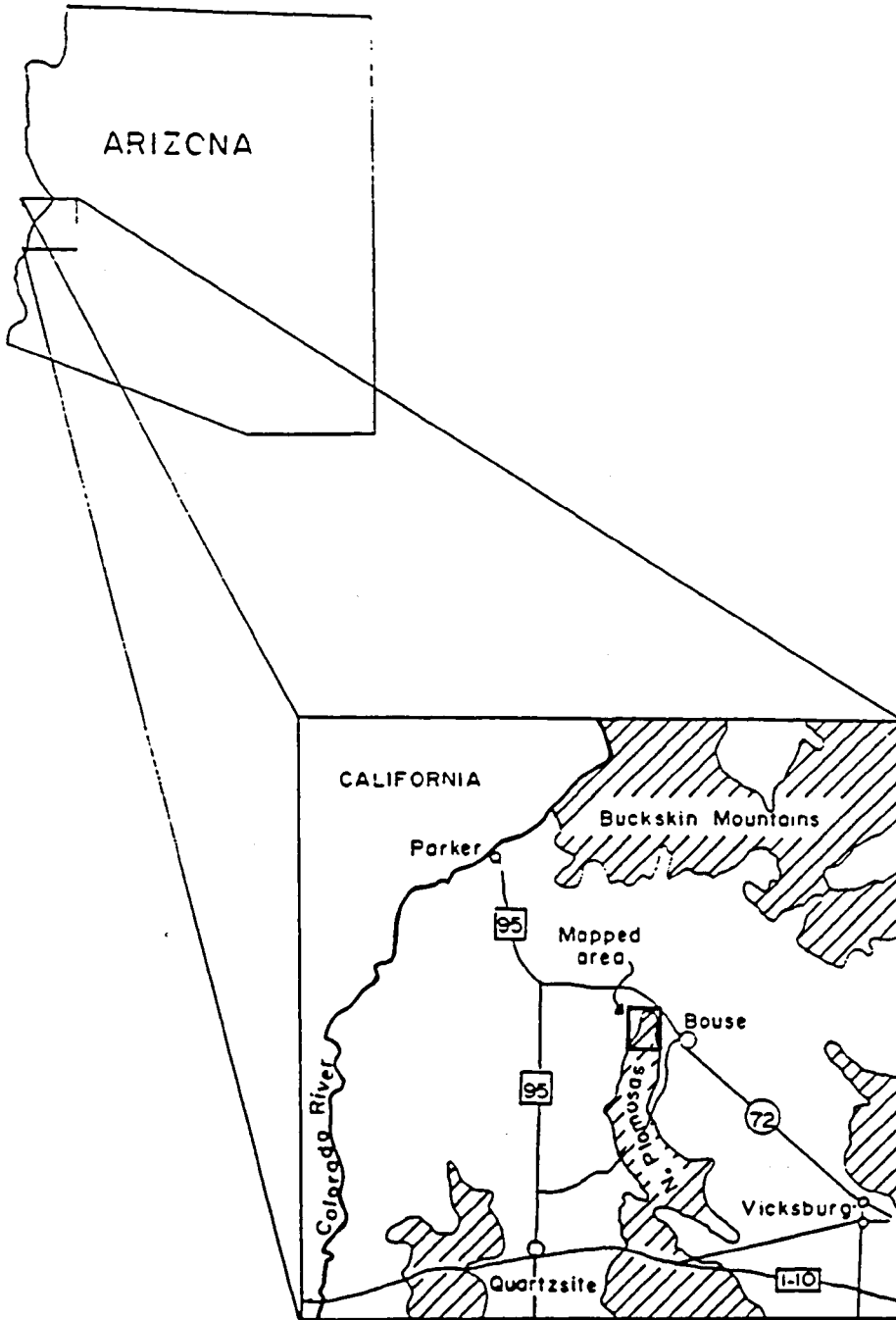


Figure 1- location of study area

accumulations of Miocene to Recent conglomerates and unconsolidated sediments. The valleys adjacent to the Northern Plomosa district are the La Posa Plain to the west and Cactus Plain to the north and east. The plains slope very gently away from the mountains at an elevation of approximately 250 meters. The Northern Plomosa Mountains reach a maximum elevation of slightly less than 600 meters. The highest point in the area of this study is Round mountain, at an elevation of 464 meters.

Climate and Vegetation

The Northern Plomosa Mountains and the area around are a true desert region. Precipitation is rare and occurs predominantly in the form of heavy thunderstorms during the months of July and August. Summers are very hot, with daily high temperatures typically over 40°C. Winters are pleasant and warm, with only occasional rain and cool weather. Vegetation is sparse and typical of the Sonoran Desert. Saguaro, cholla, and prickly pear are the most abundant cactus varieties. Ocotillo also occupies the outcrop areas, whereas greasewood and palo verde are most abundant on the plains. Large ironwood trees can be found in the larger washes; and they provide the only significant shade in the area. Grasses are virtually absent, and large areas are without any vegetation whatsoever. Dark, manganese oxide-stained "desert pavement" covers much of the non-outcrop area. In spite of

the extreme aridity of the region, ground water is relatively shallow and abundant, supplying the domestic purposes of the community of Bouse, and permitting considerable agriculture on the plains to the east. Many of the deeper workings in the Plomosa district are water-filled.

History

Howland Bancroft (1911) published the first descriptions of the mines, prospects, and geology of the Plomosa district following a visit to the area in 1909. At the time of his visit the district was being actively prospected, and had apparently been so since the latter part of the 19th century. Two mines, the Little Butte and the Blue Slate, were in operation. The target of the prospecting and mining was a hematitic breccia found within high-angle structures and carrying good values in copper and gold, with minor silver. Production in 1909 from the Little Butte mine totaled 22 carloads (approximately 900 metric tons) at a reported grade of 7.6% Cu, \$6.65/ton in gold and 2.4 oz./ton silver (Bancroft, 1911). Since the reconnaissance report of Bancroft (1911), only one specific and detailed study of the economic geology of the Northern Plomosa district has been made available to the public. J.P. Jemmett (1966) completed a doctoral dissertation in which he mapped the geology of the Linskey Northeast 7½ minute quadrangle and assessed the economic potential of the area. Scarborough and Meader (1989)

mapped the Northern Plomosa Mountains in 1981 and produced an open file report on their work for the Arizona Bureau of Geology and Mineral Technology (Scarborough and Meader, 1982). This work was of a reconnaissance nature and did not concentrate on the mineralization of the area.

Jemmett listed twelve named mines which were developed in the district after the time of Bancroft's visit; most of those listed are within the area mapped in the course of this project. In addition to the named mines, innumerable prospect pits pock the district. Virtually all of this work was apparently done in the first half of this century.

The only relatively modern mining activity of commercial scale in the district was an attempt by the Loma Grande Mining Company to recover gold values from low grade ore mined by an open pit near the old Little Butte mine. The cyanide leaching operation failed in 1960 (Jemmett, 1966). Relics of this operation, including large steel cyanidation vats, are still in evidence. At the time of Jemmett's study, the Dutchman mine was being worked at a very small scale for free gold which was sold as specimens (Jemmett, 1966). Total production from the district to date has been estimated by Keith et al. (1983) at 346,000 lbs. Cu, 5000 oz. Au, 25,000 lbs. Pb, and 7000 oz. Ag from approximately 7500 tons of ore.

Jemmett's (1966) study was part of an evaluation of the economic potential of the area by the Ruby Mining Company;

since then the district has attracted continued interest from prospectors and mining companies. Exploration of the district took on greater vigor with the rising gold prices of the 1970's and 1980's, and is very active at this time. The recent discovery and development of the Copperstone Gold mine north of Quartzsite has spurred even more intense exploration interest in the area which is the subject of this study. The Copperstone deposit is similar to the Northern Plomosa district in both mineralization and geologic setting (Spencer, et al., 1988). The Homestake Mining Company, which supported this work, is only one of several major companies presently or recently working in the immediate area of the Northern Plomosa district.

Purpose of this study

Since the publication of Jemmett's (1966) dissertation, considerable progress has been made toward an understanding of the geology of western Arizona, particularly with respect to the tectonics and structure. Recent work by the Arizona Geological Survey and others has established the presence of widely exposed, large-displacement low-angle normal faults, known as detachment faults, in western Arizona, including the Northern Plomosa Mountains (e.g. Coney, 1980; Spencer and Reynolds, 1989b). Recent studies have characterized a previously unrecognized style of mineralization that is spatially and temporally related to detachment faulting

(Wilkins and Heidrick, 1982; Spencer and Welty, 1985; 1989).

The purpose of the present study is to develop a modern understanding of the geology of the Northern Plomosa district as part of the regional geologic mapping and related studies being carried on by the Arizona Geological Survey. A further aim is to provide a more detailed and scientific characterization of the process of mineralization in the district. The Northern Plomosa district was selected for study because of its structural similarity to the nearby Copperstone district, which is expected to yield about 500,000 ounces of gold in the 1980's and 1990's.

Methods

An area of approximately 23 km² comprising the most productive part of the Northern Plomosa district, and including all or part of sections 5,6,7,8,17,18,19 and 20; T.7 N., R.17 W; and sections 1,12,13 and 24; T.7 N., R.18 W. was mapped and compiled at a scale of approximately 1:9318. The mapping included geology, structure, mineralization and alteration. It should be noted that whereas the present mapping is at a larger scale and includes more detail than Jemmett's (1966), his map was used as a basis for the present work and is quite accurate in its depiction of most of the rock types and contacts. The local names that he assigned to units of the Tertiary stratigraphic section are carried forward here. The most important changes presented here are

in interpretation and emphasis.

In the course of mapping the district, samples were collected for laboratory study. Seven examples of fine-grained igneous rocks of the area were subjected to whole-rock and trace-element geochemical analysis. Thirty samples of hydrothermal mineralization or altered rock were analyzed for eight ore and indicator metals. Eleven samples of hydrothermal barite were analyzed for sulfur and oxygen isotope characteristics, and ten samples of sedimentary and hydrothermal carbonate were analyzed for carbon and oxygen isotopic values. Finally, thirteen samples of amenable hydrothermal mineralization were subjected to petrographic and fluid inclusion study.

CHAPTER 2

Geology

REGIONAL GEOLOGY

The Northern Plomosa district is located within the Basin and Range Province of southwestern North America. The physiography and structural geology of this region was shaped largely by Cenozoic extension.

Notable regional geologic features in western Arizona include large expanses of foliated high-grade metamorphic rocks of variable and commonly obscure protolith (Spencer and Reynolds, 1989a). These rocks were generally originally mapped as Proterozoic in age owing to their highly deformed nature and metamorphic grade (eg. Wilson, 1960; Wilson et al., 1969), but have been reinterpreted in recent years based largely on new geochronologic data (Wright et al., 1986; Bryant and Wooden, 1989). The schists are commonly green in color owing to contained chlorite, and they typically have a gently dipping mylonitic fabric that is strongly and consistently lineated with a northeast trend. The metamorphic

rocks are commonly bounded above by a low-angle detachment fault that is oriented grossly parallel to the foliation in the footwall metamorphic rocks, and that places relatively unmetamorphosed upper-plate rocks of various ages, in many cases Tertiary, in contact with the lower plate. The upper-plate rocks are commonly, but not invariably, broken up by numerous normal faults that merge into, or are truncated by the underlying detachment fault. The result is a number of distinct tilt blocks which dip generally southwest into the detachment fault. The detachment fault itself is commonly underlain by a thin (<1 meter) microbreccia ledge.

Detachment faults were first recognized in the early 1970's (eg. Coney, 1974; Shackelford, 1976; see Spencer and Reynolds 1989a for a brief history and other references), but were not generally understood until the 1980's. The current generally accepted understanding of the features is that they represent large-displacement, low-angle normal faults. Mylonitic fabric in lower-plate rocks formed by ductile shearing downdip from the original detachment fault, and were uncovered by continued fault movement (Wernicke, 1981; Davis, 1983; see Figure 2). Mylonitic lineation indicates the direction of extension, and asymmetric mylonitic petrofabrics indicate that the sense of shear during mylonitization was top to the northeast in west-central Arizona (Spencer and Reynolds, 1989b). Mapping by Lucchitta and Suneson (1981)

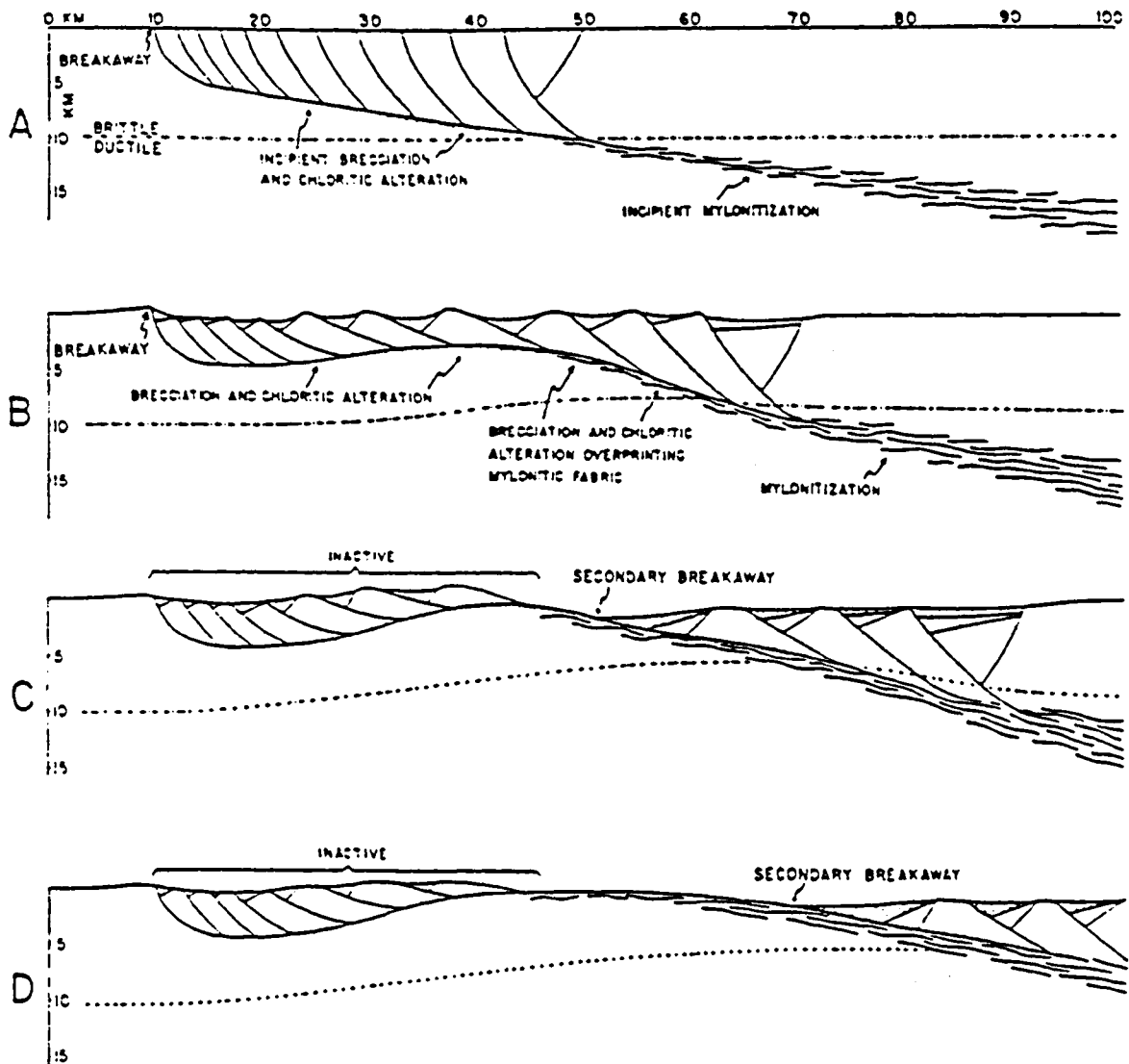


Figure 2- Generalized cross-section of a detachment fault, after Spencer and Reynolds (1989b).

indicates that the upper plate rocks to the Buckskin-Rawhide detachment fault, exposed in southernmost Mohave County, Arizona, are in fact structurally continuous with the undisturbed rocks of the Colorado Plateau. This leads to the interpretation that the lower plate was in fact pulled out from under the upper plate during the southwest-directed extension. Minimum total displacements have been estimated at 55 km on the Buckskin-Rawhide fault (Spencer and Reynolds, 1989b) and 40 to 50 km on the correlative Bullard detachment fault (Reynolds and Spencer, 1985).

Lower plate crystalline rocks, though commonly overprinted by Tertiary mylonitization (Wright et al., 1986; Bryant and Wooden, 1989), represent pre-Tertiary rocks that were at deep crustal levels before extension. Upper-plate rocks include crystalline rocks of Proterozoic age, remnants of deformed Paleozoic sedimentary rocks, Jurassic volcanic and sedimentary rocks, and early- to middle-Tertiary sedimentary and volcanic rocks (Spencer and Reynolds, 1989a). High-angle block faulting has somewhat fragmented the older geologic picture, and late Tertiary and Quaternary volcanic and sedimentary cover further obscure it.

NORTHERN PLOMOSA DISTRICT GEOLOGY

Structural Basement

The structural basement of lower-plate chloritic rocks is exposed only in the extreme southwest corner of the mapped area (See plate 1). The lower-plate rocks are distinctly green in color and generally gneissic in texture with white banding in the mapped area. They are not notably lineated except for a small area in a wash in the southwest corner of section 19, within a few tens of meters of the detachment fault, where lineations within foliation surfaces trend N40E and plunge approximately 20°. The lower-plate rocks have not been studied in detail here; they are mapped simply as lower-plate metamorphics (lpm), and considered to be the crystalline basement to the area. They continue to the south out of the mapped area to form the bulk of the Northern Plomosa Mountain Range (Jemmett, 1966).

Plomosa detachment fault

The low angle normal fault separating the lower-plate metamorphics from the various upper plate rocks was termed the Plomosa fault by Scarborough and Meader (1982), and that name is carried forward here. The detachment fault itself is not well exposed in the mapped area, but is readily recognizable where it is exposed (Figure 3). There is no characteristic silicified breccia ledge; only a thin (1 to 2



Figure 3- Outcrop of the Plomosa detachment fault in the north half of section 19. Hammer is resting on the lower plate metamorphic rocks. Upper plate is Proterozoic crystalline rock.

meter) zone of crushed rock separates lower plate chloritic rocks from the upper plate. The fault is located primarily as the easterly and northerly edge of the outcrop of lower plate metamorphics. Its orientation can be inferred in gross from the outcrop patterns, and perhaps more precisely from the orientation of the ramp of lower-plate rock taken to be the erosionally exposed footwall of the detachment. This ramp slopes at about 20° to the northeast (Figure 4).

Upper-Plate Rocks

Proterozoic Crystalline Rocks

The oldest upper-plate rocks in the mapped area are variably foliated and lineated crystalline rocks that are probably equivalent to the (1650 - 1800 Ma) intrusive and metamorphosed sedimentary and volcanic rocks identified as Xm, Xms and Xmv, respectively, on the Geologic Map of Arizona (Reynolds, 1988). Whether the protolith was intrusive or volcanic/sedimentary rock is in many places not clear, but granitoid rocks are predominant in most areas. Foliation is variably developed and in many areas is largely or entirely absent. Lineations are rare. In general, the rocks appear to be slightly to moderately deformed granitic intrusive rocks. Jemmett (1966) interpreted these granitoids to be local areas of anatectic melting within high-grade metamorphic rocks.

Several features of the Proterozoic crystalline rock



Figure 4- Ramp of lower plate metamorphic rocks (horizon in right half of photo) approximating detachment fault surface. View is looking southeast toward Round Mountain.

provide evidence that it has suffered multiple episodes of deformation in its history. Lenses and pods of white bull quartz are common throughout the Proterozoic crystalline rocks. These masses vary in size from a few centimeters to over ten meters long but are not continuous or linear in the nature of veins; nor do they have any observed preferred orientation. Jemmett (1966) interpreted the quartz bodies to be the result of metamorphic segregation; that interpretation is supported here. They are clearly earlier than the main phase of hydrothermal mineralization hosted by the Tertiary rocks, as the quartz lenses are cut by the Proterozoic-Tertiary depositional unconformity.

Dikes and irregular bodies of mafic rock are also common throughout the Proterozoic crystalline rocks. Both basaltic and diabasic textures are present in these bodies, and they are in some cases linear and dike-like over short distances. The mafic bodies cut, and are therefore later than, the bull quartz, but like the quartz lenses they are discontinuous and apparently randomly oriented. It seems likely that these in fact represent basalt and diabase dikes that have been fragmented and scattered during subsequent deformation. The individual fragments, however, must have maintained their integrity; at the mesoscopic level these rocks are commonly mineralogically and texturally fresh and undeformed.

Further impeding a clear understanding of the Proterozoic

rocks are effects associated with the thrust emplacement of a large block of Paleozoic sedimentary rock that makes up the bulk of Round Mountain and the tops of several smaller hills in the Northwest quarter of section 19 and the southwest quarter of section 18. Proterozoic rocks are foliated on the northwest flank of Round Mountain within approximately 50 meters vertically of the thrust contact with the structurally overlying Paleozoic rocks. The Proterozoic has taken on a linear tectonic fabric. Foliation is approximately parallel to the thrust contact, and Lineations within foliation planes trend S10W-S20W and plunge at 20 to 50 degrees. The lineated foliation is also well defined and consistently oriented in the northwest quarter of section 19 beneath the eroded thrust plate. In this area, the basement rocks crystalline rocks are fine grained and variably lineated, and contain red carbonate layers, some isoclinally folded, which in several cases have flat upper surfaces and irregular lower surfaces (Figure 5). The characteristics of these layers suggest that they represent original sedimentary carbonate beds, perhaps of volcanigenic exhalative origin. In the same area, subtle light-dark color contrasts within the crystalline rock seem to parallel the carbonate bands and hint at compositional layering within the protolith. These apparently sedimentary features occur only within the tectonized Proterozoic basement rocks, and are generally not strongly discordant with



Figure 5- Folded carbonate sliver in tectonized Proterozoic basement. The clipboard is directly below an isoclinal fold with closure to the upper left. A second fold nose is at the right edge of the photograph. The carbonate layer can be seen trending along the wash in the background and the foreground.

lineation. Paleozoic carbonate rocks are interleaved into basement crystalline rocks in several locations in the same area, and all the features described may in fact have been produced tectonically.

Paleozoic and Mesozoic Rocks

The Paleozoic rocks within the mapped area are complexly deformed and slivered. The only large exposure of Paleozoic rock in the study area is at Round Mountain (Figure 6). It is in thrust fault contact with underlying tectonized Proterozoic rocks, and shows abundant evidence of thrusting, shearing and slivering within the block as well. The Round Mountain block was mapped in detail by Stephen J. Reynolds of the Arizona Geological Survey, and the following description is based on his notes.

Two major thrusts within the Round Mountain block separate the Paleozoic rocks into three tectonic plates (see Figure 7). The lowest plate of Paleozoic sediments consists of a sheared but essentially intact stratigraphic section of Cambrian Bolsa Quartzite and Abrigo Formation overlain by the Devonian-Mississippian Martin/Redwall Formation carbonates, which are in turn overlain by Pennsylvanian Supai Group sediments.

The Bolsa Quartzite exposed on Round Mountain is a white to gray vitreous quartzite or arkosic quartzite which weathers



Figure 6- The Round Mountain thrust block viewed from the northwest. The basal thrust placing Paleozoic sedimentary rocks over Proterozoic crystalline basement is visible as the line of shadow at the slope-break.

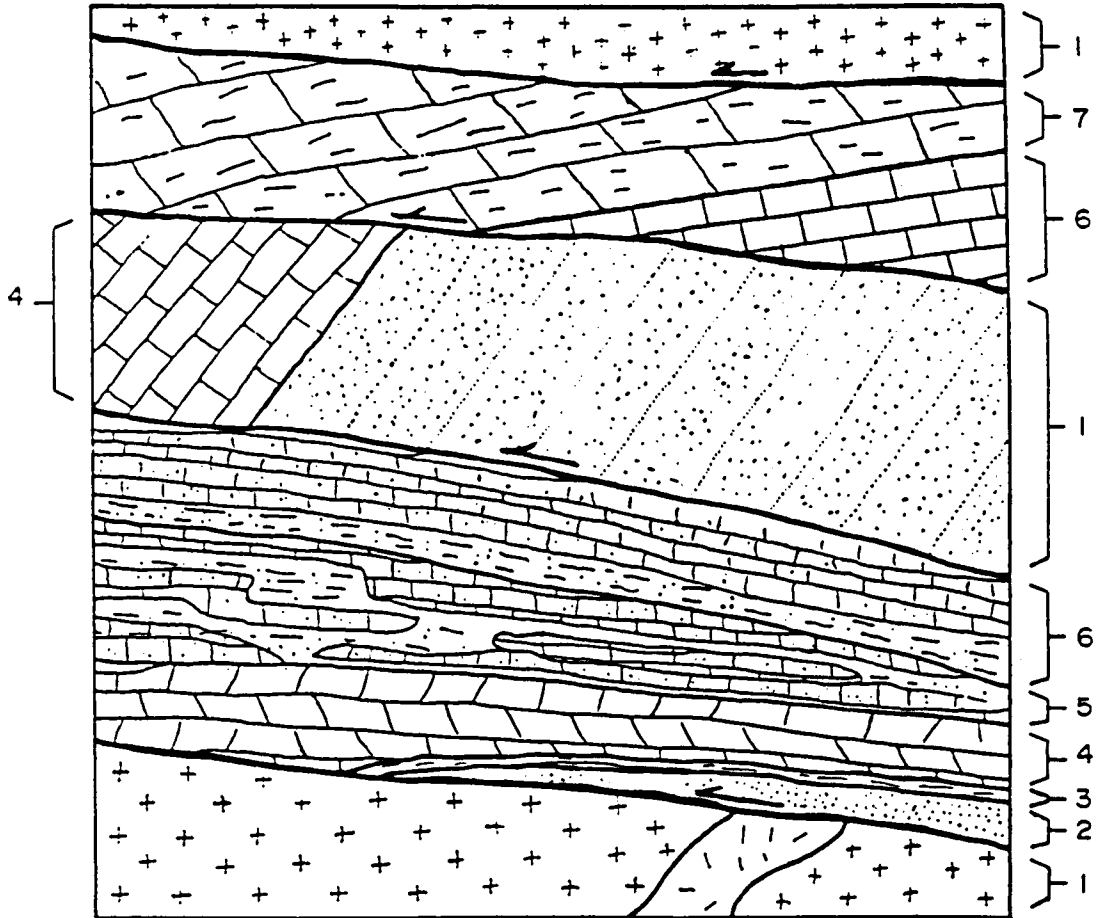


Figure 7- Structural section of the Round Mountain thrust block, as interpreted by Stephen J. Reynolds of the Arizona Geological Survey. 1. Proterozoic basement; 2. Cambrian Bolsa Quartzite; 3. Cambrian Abrigo fm.; 4. Mississippian-Devonian Martin/Redwall Fms.; 5. Pennsylvanian Supai Group; 6. Permian Kaibab fm.; 7. Triassic Buckskin fm.

to a pinkish tan. The Abrigo Formation is a thin (2-3m) silvery gray arkosic schist which separates the Bolsa Formation from the overlying Martin Formation, a poorly bedded tan to brown dolomite. The Redwall Formation takes the form of a medium-bedded cherty gray limestone. The Martin and Redwall together are about 30 meters thick. The overlying Supai Group consists of thin- to medium-bedded pink to maroonish gray shales, arkoses and calcareous sedimentary rocks.

Stratigraphy and shearing in this lower plate of sedimentary rocks are approximately parallel to the contact with the Proterozoic basement, and to foliation in the basement rocks. The lower contact of this package with the Proterozoic basement is a fault, rather than simply a sheared depositional contact, as evidenced by the slight discordance of the contact with stratigraphy. The Bolsa Quartzite thins and eventually disappears along the strike of the contact to the southwest, where Martin/Redwall carbonates are in contact with the underlying crystalline rocks.

A second, structurally higher, thrust fault places Bolsa Quartzite over the Supai Group of the underlying plate. The Bolsa Formation of this middle plate is markedly discordant with the underlying fault and stratigraphy. In places the bedding in the quartzite dips essentially vertically, and at high angles to bounding faults above and below. The

anomalously thick and probably thrust-repeated section of steeply dipping Bolsa Quartzite is traceable southward along the eastern side of Round Mountain to its depositional contact with the overlying Martin/Redwall Formation carbonates. This relationship indicates that stratigraphic tops are to the south or southeast.

A structurally higher thrust fault places approximately 35 meters of variably bedded and cherty gray to brown limestone and dolomite of the Permian Kaibab formation over the steeply dipping strata of the middle plate. Bedding in Paleozoic strata of this upper plate dips approximately 60° to the south, slightly more steeply than the underlying fault contact. In the southeast corner of Round mountain, dark brown carbonates and calc-silicates of the Triassic Buckskin formation lie positionally above the Kaibab formation. Farther west, however, the Kaibab Formation is bounded above by a fourth low-angle fault which places Proterozoic Basement over the top of the entire sedimentary package.

In addition to the large exposures on Round mountain, thrust klippe of Paleozoic rocks crop out above tectonized Proterozoic basement in the northwest corner of section 19 and the southern part of section 18. These areas were mapped by the author as undifferentiated Paleozoic carbonate and quartzite (PZc and PZq).

Tertiary Stratigraphy

Lying depositionally on the Proterozoic crystalline rocks in the vicinity of the Northern Plomosa district is a well exposed, well defined and reasonably continuous section of Tertiary sedimentary and volcanic rocks, which occupies approximately half of the mapped area. The section (Figure 8) is floored by a basal conglomeratic arkose that grades upward into finer grained arkoses, thin-bedded silty limestones, and eventually thick-bedded (1 to 3 meters) limestone. The calcareous sediments are interbedded with layers of felsic tuff which become thicker and more abundant toward the top of the unit. Overlying the sedimentary section in apparent conformity is a thick layer of mafic to intermediate volcanic flows, flow breccias, and agglomerates, with minor interbedded sediments and tuffs. The uppermost unit in the Tertiary section is a coarse, heterogeneous, crudely stratified to unstratified conglomerate that was deposited with apparent disconformity onto the underlying volcanic unit. Minor Tertiary felsic intrusions intrude the Tertiary sediments and the underlying Proterozoic basement and Paleozoic metasediments.

The Tertiary strata were mapped and described by Jemmett (1966) and Scarborough and Meader (1983, 1989). In both studies the Tertiary section in the northern Plomosa Mountains was correlated with the Artillery Formation defined

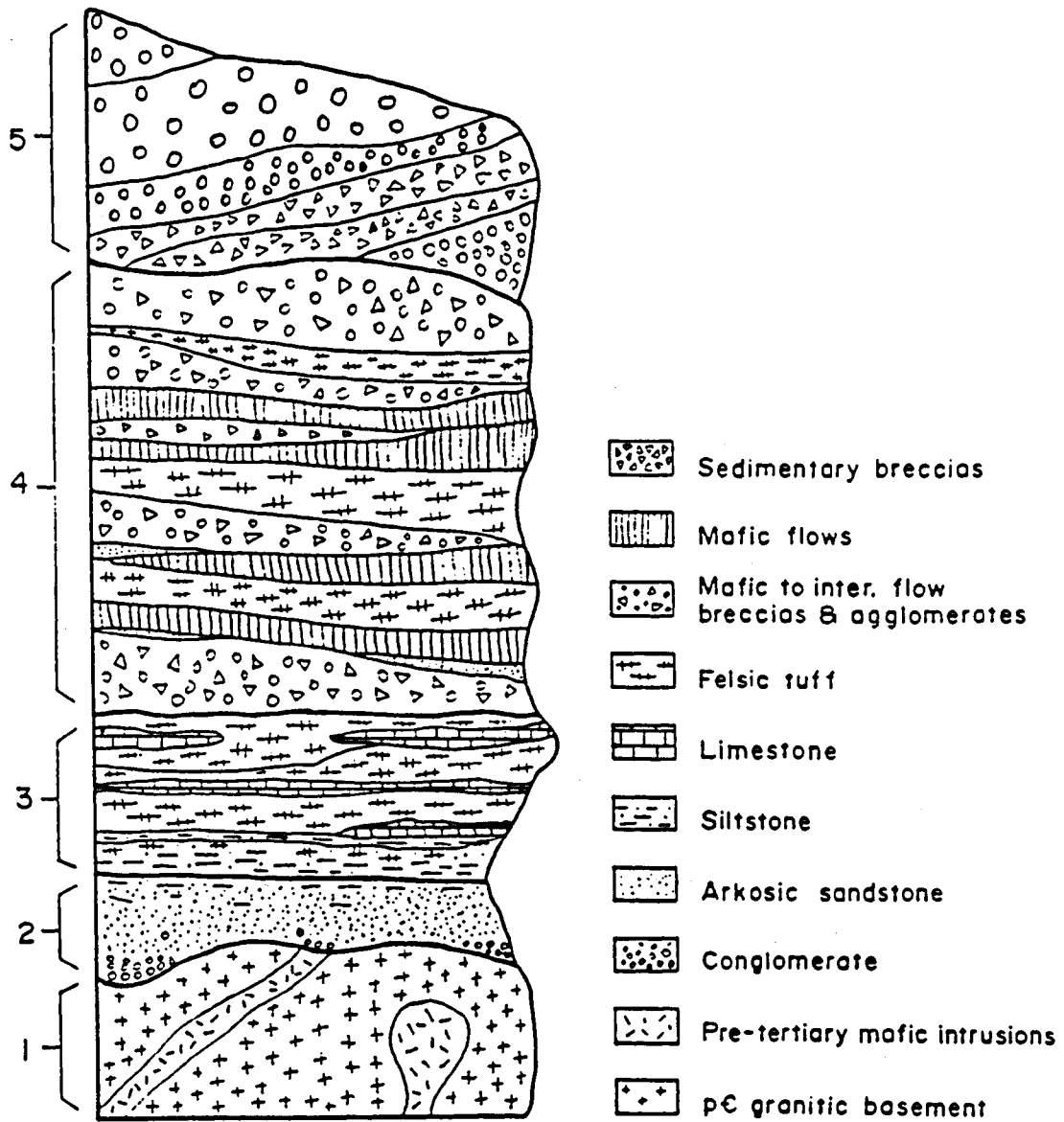


Figure 8- Tertiary stratigraphy of the Northern Plomosa district. 1. Proterozoic basement, 2. Bouse arkose, 3. Limestone-tuff unit, 4. Volcanic unit, 5. Plomosa conglomerate.

by Lasky and Webber (1949) and located approximately 60 km to the northeast, but this correlation is considered speculative and is not addressed further here. Local unit names used by Jemmett (1966) are used here; Bouse arkose (Tba) for the lowermost unit, and Plomosa conglomerate (Tpc) for the top unit, are used here. The calcareous sediments were mapped as a single limestone-tuff unit (Tlst) in most cases, and broken out into separate Tertiary limestone (Tls) and felsic tuff (Tvt) units where possible. The overlying mafic to intermediate volcanic pile is undifferentiated and given the map symbol Tv.

Bouse Arkose

The Bouse arkose lies depositionally upon an irregular erosional surface above the Proterozoic basement rocks, and consists of a discontinuous basal boulder conglomerate which fines progressively upward into pebble conglomerate and finer grained arkosic sandstones.

The basal boulder conglomerate varies in thickness from 0 to over 20 meters and consists of pebbles to boulders (up to 1 meter diameter) of the underlying Proterozoic crystalline rock, as well as cobbles and pebbles of Paleozoic sedimentary rocks and various rock types which are dissimilar to local units, with a matrix of arkosic sand. The thick boulder conglomerate lenses apparently accumulated in channels cut in the underlying Proterozoic crystalline rocks. Above the

boulder conglomerate, or where it was not deposited, a thin pebble conglomerate grades over a few centimeters to meters into a light-gray, friable, coarse arkose with local suspended pebbles. The arkose commonly becomes richer in iron as it fines upward, resulting in a chocolate brown color for the upper part of the arkose unit. Iron content remains high as the arkose grades into the orange calcareous siltstones above.

Limestone-tuff Unit

The lower contact of the calcareous sediments is marked by the upward occurrence of sharply defined bedding and lamination. In the lower parts of the limestone-tuff unit the rocks are laminated or thinly bedded (1-5 cm), giving the rocks a shaley appearance. Very little shale actually exists in this unit, however. The unit is dominated by thin bedded silty limestone with silty partings. Interbedded with the limestone are thin layers (1-5 cm) of felsic tuff. Jemmett (1966) identified these layers as devitrified welded tuff on the basis of his petrographic work. At progressively higher stratigraphic levels the orange calcareous unit is decreasingly silty and the tuff layers are more abundant and thicker (see Figure 9). The color of the unit correspondingly changes from orange to brown. The carbonate layers also become progressively thicker upward in the section; owing in part to partial silification, the thicker limestone beds have a mottled gray color and weather to a rough brown surface.

In the long, well exposed section in the south half of section below, the unit is capped by a relatively thick (3-5 meters) and continuous layer of the gray limestone.

In the southern part of the mapped area, however, especially in the area northeast of Round Mountain, tuff is



Figure 9- Limestone-tuff unit. Orange thin-bedded to laminated T1st is in foreground; thicker limestone (gray-brown) and felsic tuff layers near the top of the unit are visible in the background.

In the long, well exposed section in the south half of section seven, the unit is capped by a relatively thick (2-3 meters) and continuous layer of the gray limestone.

In the southeast part of the mapped area, however, especially in the area northeast of Round mountain, tuff is the dominant lithology and the gray limestone exists as discontinuous bodies in and on the thick tuff layers. The discontinuous nature of the capping limestone in this area is in large part due to dismemberment by faulting. In some parts of the mapped area the exposures of limestone are sufficiently large and discrete, and the enveloping tuff sufficiently voluminous that the rock types are mapped separately. An extrusive center to the east is suggested by the varying abundance of tuff in the T1st unit. Some evidence for this can be seen in the northeast quarter of section 19. In the washes immediately north and east of Round Mountain a sill of white felsite intrudes Bouse arkose and inflates the section.

Volcanic Unit

Overlying the limestone-tuff unit without obvious disconformity is a thick section of volcanic flows, flow breccias, and agglomerates, with minor interbedded volcanoclastic sediments. The textures and compositions of the volcanic rocks vary considerably. Vesicular and amygdaloidal basalt or andesite flows are common, especially in the western exposures in the mapped area, but the bulk of

the volcanic section is composed of agglomerates and flow breccias ranging in composition from intermediate to mafic. The agglomerates exposed in the eastern portion of the district are markedly more felsic in appearance than those to the west. Some white rhyolitic flows and tuffs are included in the volcanic pile, as are thin (up to 1 meter) beds of red, arkosic, volcanoclastic sandstone.

The volcanic section is stratigraphically quite complex and is further complicated by faulting. Due to this complexity, the volcanic section is mapped as a single unit. Its total thickness could be greater than 300 meters.

In gross the volcanic section is the darkest unit in the mapped area, and is recognized easily from air photos or any elevated vantage point. Over most of the district, the volcanic rocks are deep red to maroon in color owing to abundant contained hematite, but the more felsic agglomerates in the eastern part of the area of interest weather to brown.

Only a small minority of the rocks of the volcanic section are fresh in appearance and pristine in their mineralogy. In most instances, the only identifiable minerals are hematite, potassium feldspar, and quartz, with or without calcite. This is the assemblage identified by Chapin and Lindley (1986) as characteristic of potassium metasomatism, which is a common regional phenomenon in Tertiary volcanic rocks of western Arizona (Brooks, 1986, 1988; Kerrich et

al., 1989). Chemical analyses of these rocks indicate that most have in fact undergone marked enrichment in potassium.

Plomosa Conglomerate

The uppermost unit of the Tertiary section in the Plomosa district has been named the Plomosa conglomerate by Jemmett (1966). The Plomosa conglomerate is a heterogeneous coarse clastic unit that includes both clast and matrix(?) supported conglomerates and sedimentary breccias. It rests with apparent angular unconformity upon the underlying volcanics. The unit is stratified only in the crudest sense, and in most outcrops no stratification whatsoever is observed.

In the thickest section exposed in the district, the conglomerate forms much of the top of Beehive Hill in the eastern part of section 18 (Figure 10). On Beehive hill, the Plomosa conglomerate dips to the south above a northeast-dipping contact with the underlying volcanic unit. The base of the unit is composed of a boulder conglomerate consisting of large, well rounded boulders of granitic rock which Jemmett (1966) identified petrographically as perthitic granite. No granite of similar nature is found outcropping in the mapped area, however Scarborough and Meader's (1989) map of the area shows megacrystic granite cropping out a short distance north of Round mountain. The matrix of the Plomosa conglomerate is a dense hematitic mudstone that imparts the red coloration to the unit. Upward in the conglomerate the large granite



Figure 10- Beehive Hill viewed from the northeast. Plomosa conglomerate in angular unconformable contact with underlying Tertiary volcanic rocks.

boulders give way to smaller (less than 25 cm), more angular clasts of schistose rock. Some of these have quartz eyes and are identifiable as metamorphosed felsic volcanic rock.

Because it is stratigraphically the highest Tertiary unit exposed in the mapped area, and is exposed only as erosional remnants, no estimate of thickness can be made here. However, farther south in the Plomosa Mountains Jemmett (1966) noted that the Plomosa conglomerate grades upward into normal Tertiary conglomerates.

As mentioned earlier, the Plomosa conglomerate is very heterogeneous; many other exposures of the unit bear little resemblance to the section on Beehive hill, except in their coarse clastic nature and lack of good stratification. One small outcrop in the northeast corner of section 18 consists of a pile of shattered felsic metavolcanic rock. No matrix is evident, and the fragments seem to fit together as though they were once part of a single coherent mass. An apparently equivalent breccia crops out near the road immediately northeast of Beehive hill. In this area the felsic metavolcanic breccia is overlain by another member of the unit, a coarse, angular conglomerate composed entirely of clasts of Paleozoic limestone and quartzite in a calcareous matrix.

Quaternary/Recent

Bedrock outcrops in the Northern Plomosa district are covered by Quaternary and recent gravels along the east, north, and west flanks of the range, and thin sheets and tongues of Quaternary alluvium cover large areas of shallowly buried bedrock of low relief. The area seems to be experiencing a period of renewed erosion, however, as many of the tongues of Quaternary gravel are cut by active incised washes. A caliche-cemented Quaternary conglomerate developed below the steep eastern flanks of Round Mountain would cover most of the outcrop in sections 17 and 20 if projected north and east at the level and slope of the remnant exposure.

Structure

The structure of the Northern Plomosa district is complex. At least four separate structural events ranging in age from Proterozoic to late Tertiary are recognized within the rocks of the mapped area: 1) Proterozoic regional deformation, 2) Mesozoic thrusting and folding, 3) Mid-Tertiary detachment and listric normal faulting, and 4) late Tertiary Basin and Range block faulting.

The Proterozoic rocks of the district have been notably disrupted structurally, probably in more than one event. No attempt has been made here to decipher the structure of the

Proterozoic in any detail; however some clues are available as to its deformational history. The foliation in much of the Proterozoic is evidence of at least one deformation, and the quartz pods and folded carbonate rocks could be related to that same event. The intrusion and dismemberment of the unfoliated mafic dikes is evidence of at least one later, possibly Phanerozoic event.

Round mountain provides abundant evidence of a distinct era of shortening and thrusting that affected the Paleozoic rocks of Round mountain. It imparted a lineated tectonic fabric and probably interleaved the sedimentary carbonates into the Proterozoic rocks of the footwall. The deformation is interpreted to be part of a regionally recognized southeast to southwest directed polyphase folding and thrusting event which is probably Cretaceous in age. The rocks affected by this event make up the Maria Fold and Thrust Belt defined by Reynolds et al. (1986).

The most obvious consequence of deformation in the Northern Plomosa district are the many fault-bounded tilt blocks that make up the upper plate of the detachment fault. The most common tilt direction of the blocks is to the southwest and west, as determined from the dips of the Tertiary units. This tilting and rotation is evidently the result of movement along northwest- to north-striking normal faults which commonly bound the tilt blocks. Subordinate

oblique and possibly a few strike-slip faults separate the tilt blocks which apparently rotated independently.

The major structure, which almost certainly controls the block faulting and rotation, is the northwest-striking Plomosa detachment fault that cuts the southwest corner of the mapped area through sections 19 and 24, and underlies the district at depth. The strikes of the normal faults which define tilt blocks are for the most part sub-parallel to that of the detachment, and block tilting is dominantly into the down-dip projection of that structure. It is interpreted that the normal faults are listric and possibly merge at depth with the detachment fault. Oblique and strike-slip faults commonly strike northeast to east and evidently served primarily to accommodate differential displacement and rotation of the fault-bounded tilt blocks. Gentle warping of the Tertiary carbonate sediments is evident where disruption by high angle faulting is most intense. Minor bedding plane slip seems to have occurred between the thicker limestone layers and the enclosing tuffs. Both of these phenomena can be ascribed to the effects of block faulting and rotation on materials of varying competency.

Dips in the rotated Tertiary strata vary from vertical to quite shallow (10°), but concentrate in the 30 to 50 degree range (see plate 1). There is some shallowing of dip from the base to the top of the Tertiary section in individual blocks;

however, this is not perceptible in all blocks. In the most extreme example, intrusion of Tertiary felsite inflated the section probably caused at least part of the variation in dip.

The youngest well defined structural phase that can be seen in the rocks of the Northern Plomosa district is the Basin and Range event. A N10°E-striking, linear, high-angle fault offsets the detachment in the southwest corner of the mapped area. This is most easily interpreted as a normal fault with the east side downthrown. Its nature, orientation and timing are all typical of the postdetachment Basin and Range event.

CHAPTER 3

Chemistry of fine-grained igneous rocks

As was noted earlier, most of the volcanic rocks in the Tertiary section are decidedly altered, and appear to have been K-metasomatized. In an effort to verify the inferred K-metasomatism and to gain some understanding of its nature, seven samples of igneous rocks in the mapped area were collected and analyzed for major and selected trace elements (see Table 1). The rocks analyzed include three samples of the more felsic agglomerates from the south half of section 20, T7N, R17W, two samples of mafic flow rocks from the western part of the district, and two samples of mafic dike rock from the Proterozoic basement (see plate 2 for sample locations). Of these samples, all of the agglomerates and one of the mafic flow rocks (sample 11-28-11) were identified as potassically altered on the basis of mesoscopic inspection; the others appear unaltered in hand sample.

Primary chemistry and K-metasomatism

Major element chemistry confirms the field identification of K-metasomatized and fresh rock. The K/Na ratio is the

WHOLE ROCK GEOCHEMISTRY

SAMPLE#	11-28-1	11-28-4	11-28-5	11-28-1	11-28-1	11-28-6	11-28-1
	intermed. agglom.	intermed. agglom.	intermed. agglom. (w/Ba-vn)	mafic flow	mafic flow	mafic dike	mafic dike
OXIDE(wt.%)							
SiO ₂	64.60	58.50	64.10	42.00	44.10	50.00	42.70
Al ₂ O ₃	12.70	13.10	11.70	15.20	15.60	15.60	15.00
CaO	3.28	2.60	2.04	8.98	9.85	9.40	9.58
MgO	0.28	0.39	0.24	2.83	5.10	4.67	10.30
Na ₂ O	0.52	0.22	0.20	0.36	1.94	2.80	2.26
K ₂ O	9.40	11.00	8.97	9.23	3.67	1.69	1.55
Fe ₂ O ₃	4.35	9.85	9.09	10.30	9.24	8.67	9.70
MnO	0.30	0.56	0.08	0.34	0.17	0.17	0.15
TiO ₂	0.34	0.67	0.27	0.99	1.08	1.12	1.39
P ₂ O ₅	0.11	0.37	0.10	0.22	0.43	0.23	0.27
Cr ₂ O ₃	0.00	0.00	0.00	0.01	0.00	0.01	0.06
LOI	3.16	2.70	2.39	9.16	9.00	5.47	5.16
TOTALS	99.40	100.20	99.70	100.00	100.40	100.00	98.30
ELEMENT(ppm)							
Rb	230	227	234	187	77	63	108
Sr	158	81	75	436	607	491	564
Ba	2,570	1,670	4,460	2,550	1,150	658	1,050
Y	18	21	12	21	24	22	22
Nb	11	12	9	9	11	12	9
Zr	133	144	92	92	142	111	60

Table 1- Whole rock and trace element analyses of seven Tertiary volcanic and pre-Tertiary(?) mafic intrusive rocks in the Northern Plomosa district. Analyses were performed by X-ray Assay Labs in Don Mills, Ontario. Method used was x-ray diffraction on fused disks for major elements; on pressed pellets for Y, Nb, and Zr.

simplest and best established index of the degree of K-metasomatism (Brooks, 1986; Roddy et al., 1988). The metasomatized samples (samples 11-28-1, 4, 5, and 11) have K/Na values ranging from 18 to 50, whereas the unaltered rocks (samples 11-28-6, 12, and 13) have K/Na ratios of 0.60 to 1.9. These data confirm the interpretation based on field observation that the metasomatizing fluids did not reach or did not affect the mafic intrusive rocks within the Proterozoic crystalline basement, and left a small minority of the Tertiary volcanics relatively unaltered.

Figure 11 is a discrimination diagram devised by Winchester and Floyd (1977) to identify altered volcanic rocks based on relative abundances of the relatively immobile elements Zr, Ti, Nb, and Y. The more felsic agglomerates from the eastern part of the district plot near the triple-point junction of the andesite, trachyandesite, and rhyodacite-dacite fields, and the mafic flow and dike rocks all plot within the subalkaline basalt or andesite fields. Immobile element chemistry suggests these rocks were not anomalously potassic prior to metasomatism. This contrasts with the work of Kerrich et al. (1989) who, using the same criteria, inferred that most K-metasomatized rocks from a broad area of southwestern Arizona were originally alkali basalts and intermediate rocks with estimated primary K_2O concentrations of 3 to 6% .

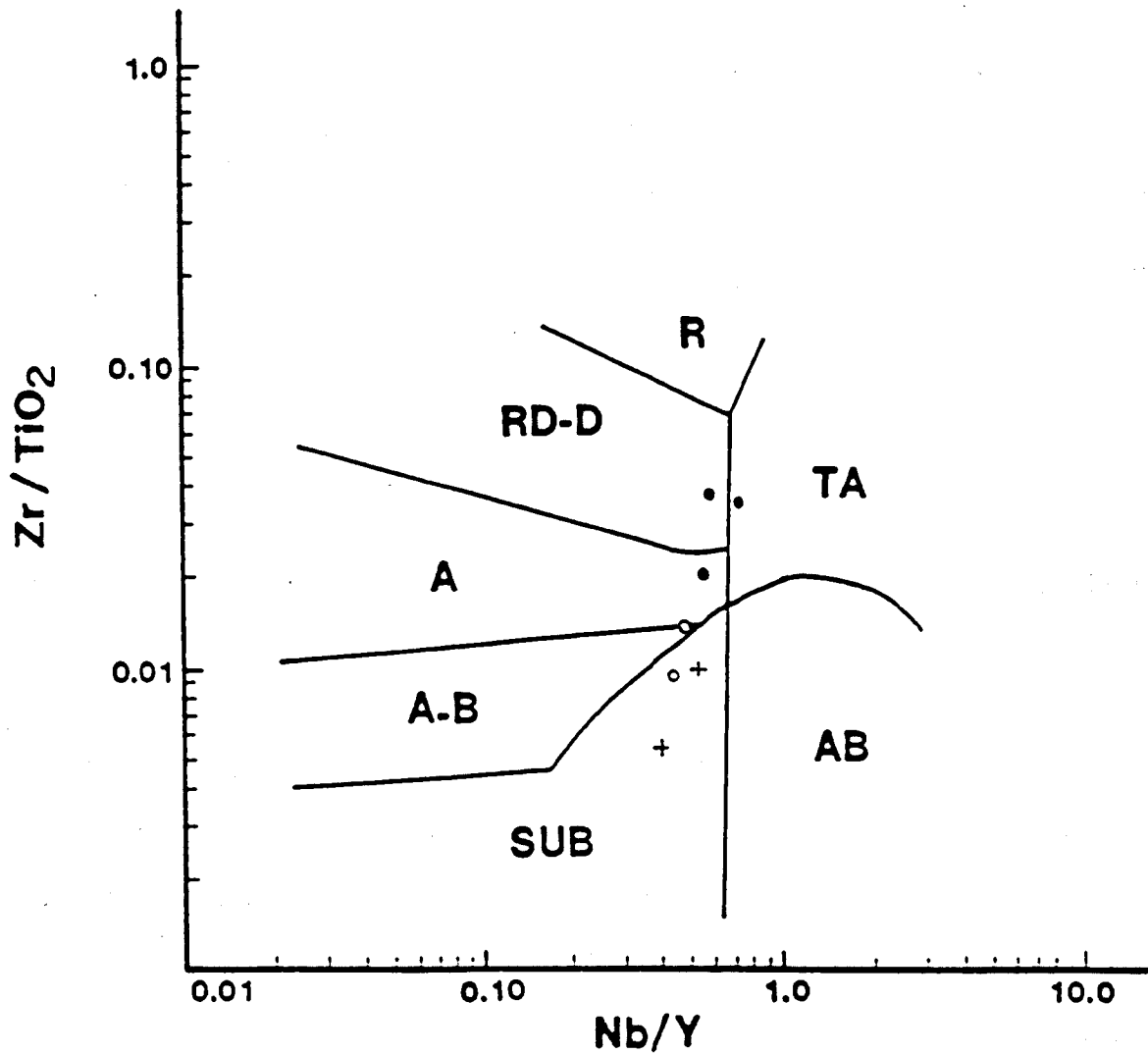


Figure 11- Discrimination diagram after Winchester and Floyd (1977). Crosses represent mafic intrusions in Proterozoic basement, open circles represent Tertiary mafic volcanic flow rocks, and closed circles represent intermediate composition Tertiary Volcanic rocks. R=rhyolite, TA=trachyandesite, AB=alkali basalt, SUB=subalkaline basalt, A-B=andesite-basalt, A=andesite, RD-D=rhyodacite-dacite.

The Winchester and Floyd (1977) classification system is dependent on the presumed immobility of Zr, Ti, Nb, and Y. Without analyses of reliably identified altered and unaltered equivalents to verify the immobility of these elements during K-metasomatism, some skepticism of the classification is justified.

Gains and Losses

The isocon diagram was developed by Grant (1986) as a way to determine chemical gains and losses affecting rocks during alteration. It is premised on the understanding that in rocks that were equivalent before alteration, a constant ratio will be maintained between immobile elements, regardless of the effect of alteration on mobile elements, or on the mass, volume or density of the rock. When chemical concentrations from major and trace element analyses of a fresh (or least altered) rock are plotted on the X-axis against those concentrations from an altered equivalent on the Y-axis, the immobile elements should, as a result of their constant ratios, plot on a straight line through the origin. This line is known as an isocon. All elements whose concentrations have been increased in the alteration process will plot above the isocon and those which have been depleted will fall below the line.

Two isocon diagrams have been constructed using the whole rock geochemical data in Table 1 in an attempt to elucidate

the chemical gains and losses caused by K-metasomatism and related(?) mineralization.

Figure 12 is an isocon diagram comparing the two mafic flow rocks analyzed, one K-metasomatized, the other relatively unaltered. Field relations and mesoscopic inspection of the two indicate that they were not precisely equivalent before alteration. However, they are geochemically similar, as evidenced by their immobile element content (see Figure 11), and are apparently part of the same mafic volcanic event. On the basis of these considerations, they are compared as "generally similar" rocks which have been affected to different degrees by K-metasomatism. Both of these samples are apparently unaffected by alteration other than K-metasomatism.

The isocon in Figure 12 is not precisely located, but is indicated by an envelope containing the generally recognized immobile elements Al, Nb, Ti, Y, and Zr. In spite of its imprecise nature, the diagram shows quite clearly the most important gains and losses brought about by K-metasomatism of these rocks; K, Rb, Ba, and Mn have all been enriched to approximately the same degree (160%), and Na has been depleted by approximately 75%. Less dramatic effects include a gain of Fe and losses of Mg and P. No inference can be made as to gain or loss of Sr, Si, Al, or Ca, except that the effects probably were not large, as they plot within the "isocon

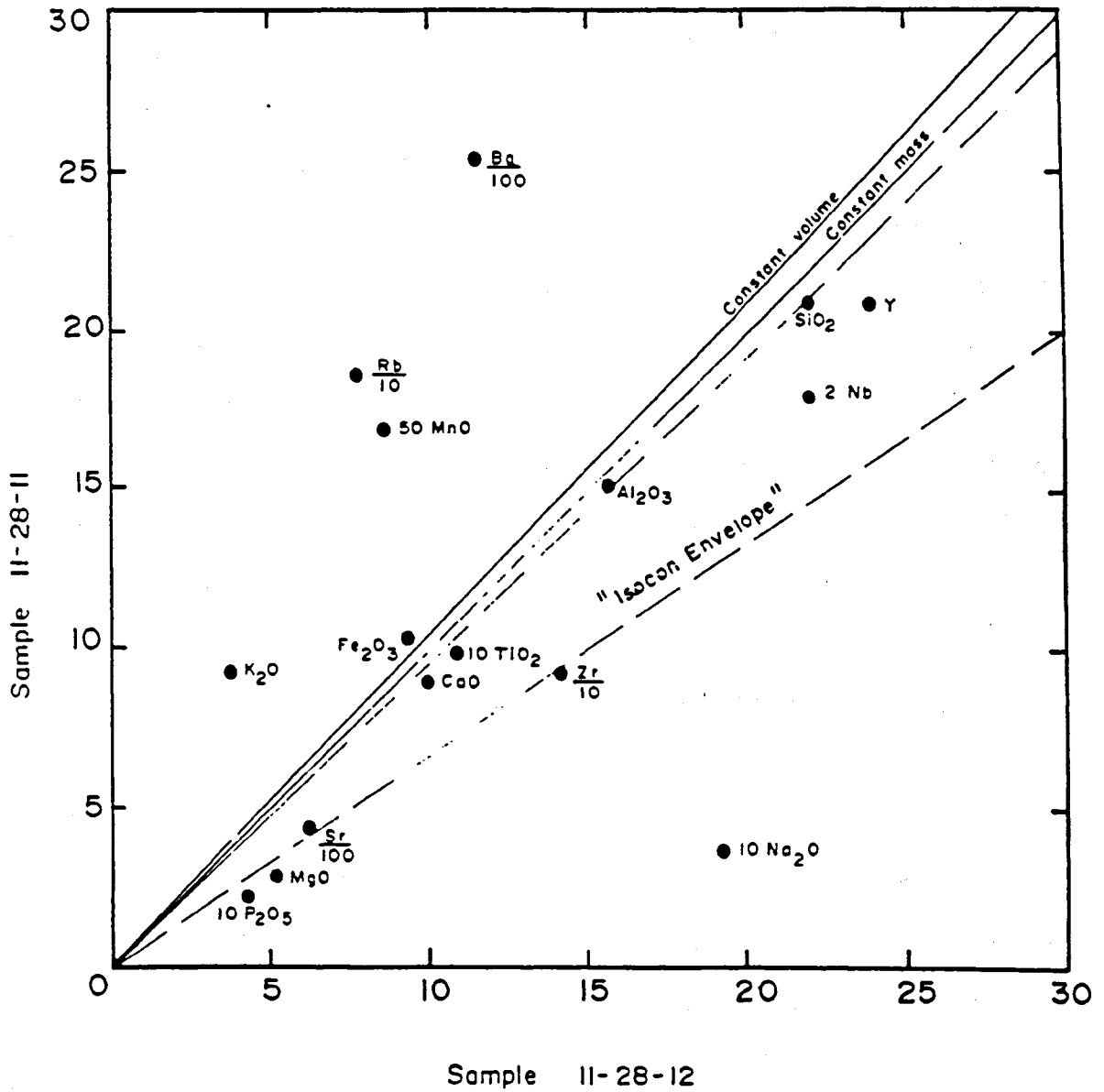


Figure 12- Isocon diagram comparing an unaltered Tertiary mafic flow rock (sample 11-28-12 with a K-metasomatized near-equivalent (sample 11-28-11).

envelope".

The gain in potassium and loss of sodium is, of course, noted in all K-metasomatized rocks, and enrichment in rubidium is also generally noted (Brooks, 1986, 1988; Roddy, 1988; Kerrich et al., 1989), however other gains and losses noted here are not all consistent with other studies of the phenomenon. Kerrich et al. (1989) did not attempt to identify gains and losses quantitatively, but did infer gains of Fe, Ca, Ba, and Mn, and a loss of Mg, in metasomatized rocks. Roddy et al. (1988) did not identify any gains other than K and Rb, but found that Ca, Mg, Sr, Pb, Zn, and Mn were depleted in K-metasomatized samples.

Figure 13 is an isocon diagram comparing two samples of the intermediate agglomerate from the eastern part of the mapped area. Field and chemical evidence suggest that these were very nearly equivalent before alteration. Both samples are K-metasomatized, but sample 11-28-5 was collected from within approximately one meter of an area of barite-hematite veining, and is presumed to have been affected by vein-related alteration. The isocon in Figure 13 has been drawn as a best-fit line through Y, Zr, Nb, TiO_2 , and Al_2O_3 . The large gains in Fe and Ba can be easily attributed to alteration around the barite-hematite veins. However, the strong depletion of Mn is less easily explained. An oxidizing solution such as that which deposited the barite-hematite assemblage would not be

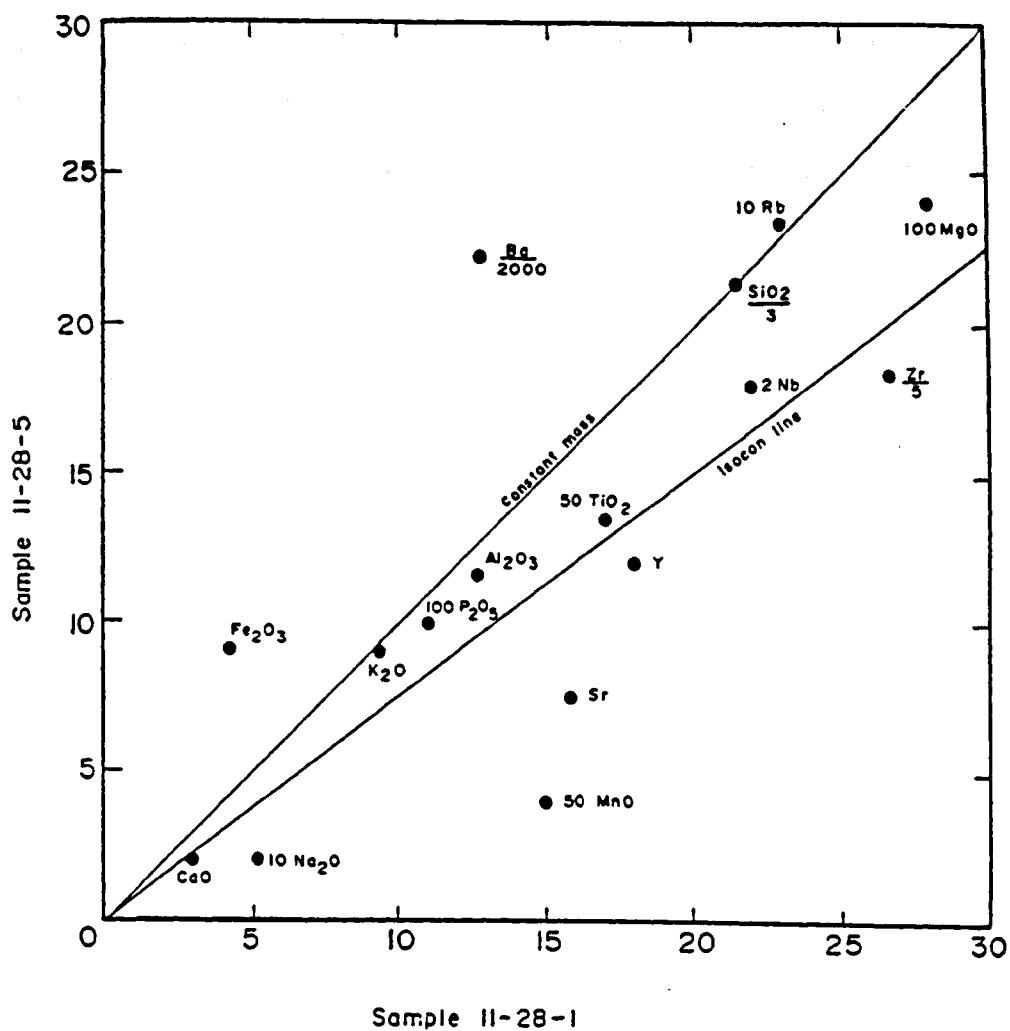


Figure 13- Isocon diagram comparing unmineralized K-metasomatized intermediate volcanic rock (sample 11-28-1) with an equivalent rock within the alteration halo of a barite-hematite vein (sample 11-28-5).

expected to mobilize and remove manganese. This suggests that a reducing fluid might have affected the rock after K-metasomatism and before the barite-hematite mineralization.

CHAPTER 4

Mineralization and alteration

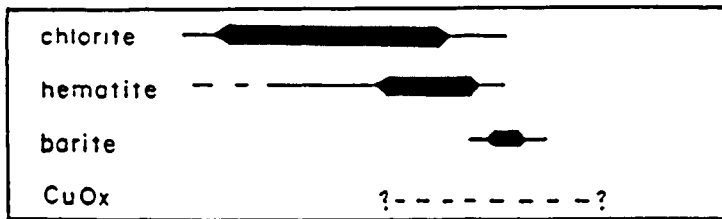
The Northern Plomosa district is an intensely mineralized area. Hydrothermal fluids have affected to one degree or another virtually all the rocks in the district. In the course of this study, outcropping mineralization and mine dump materials from dozens of locations across the district were examined, and a total of 13 thin and thick sections of hydrothermal mineralization were studied petrographically. Detailed mineral assemblage and paragenetic information was compiled for 10 locations in the area, including most of the larger mines and prospects. Individual paragenetic sequence diagrams for the different localities are provided in Figure 14. Comparison and compilation of the individual parageneses suggests that most of the mineralization can be related in a fairly consistent and well-defined paragenetic relationship representative of the district as a whole (Figure 15).

Alteration and Replacement

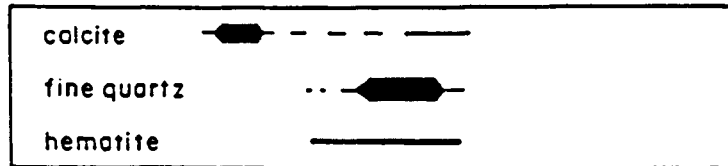
1. Chlorite stage

In the calcareous sediments, the earliest stage of

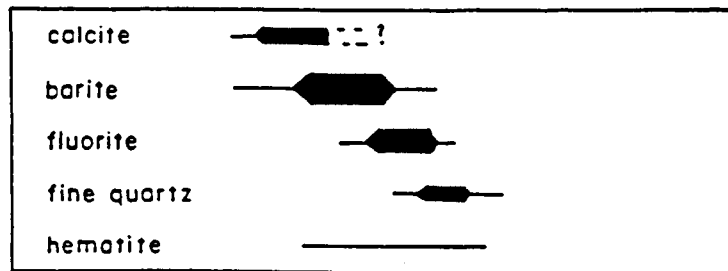
PMD-10
(Little Butte Mine)



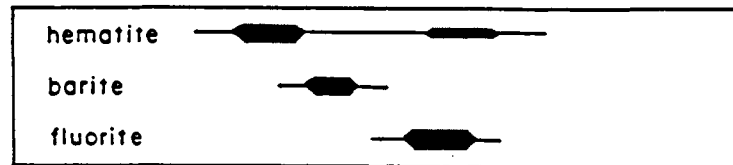
PMD-5
(Dutchman Mine)



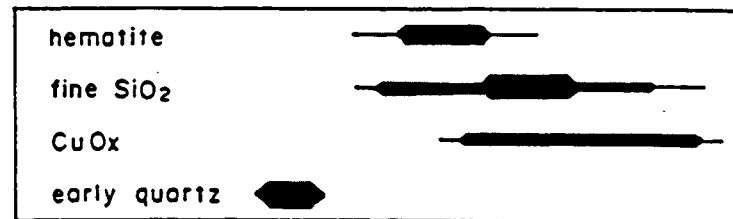
PMD-15
(Sect. 17 Ba-F1 prospect)



PMD-8
(Airstrip deposit)



PMD-9
(Arrastre Mine)



PMD-7
(Adele M. Mine)

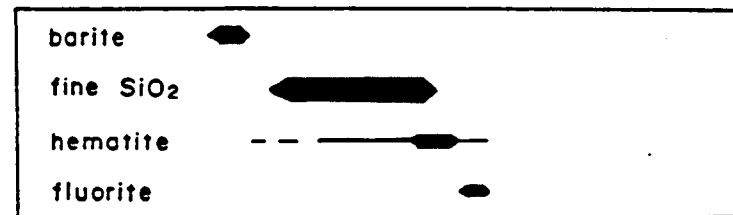
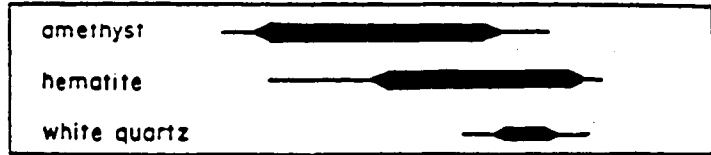
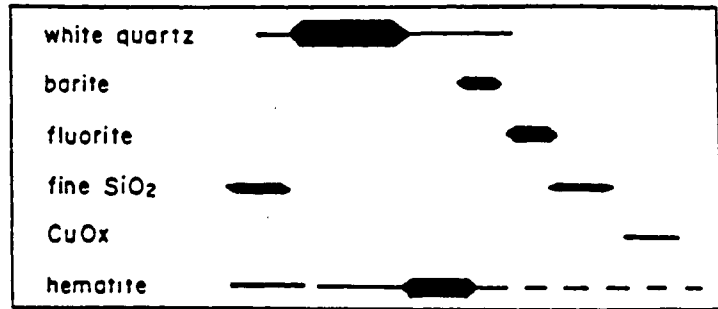


Figure 14- Paragenetic diagrams for 10 important mineralized localities in the Northern Plomosa district (see Plate 2 for locations).

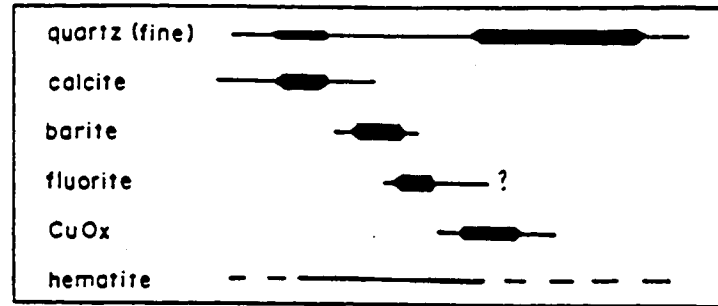
PMD-30
(Amethyst veins)



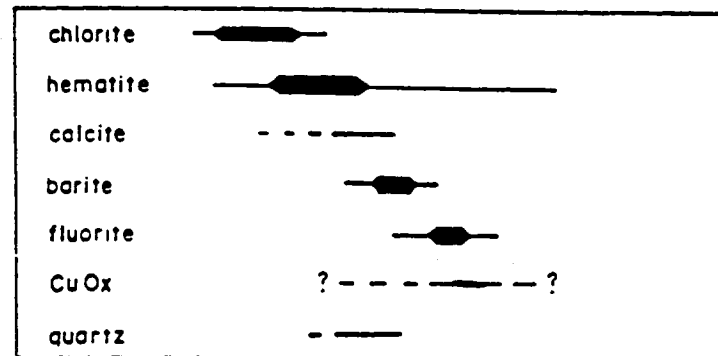
PMD-28
(Scotchman vein)



PMD-3
(BHH vein)



PMD-11
(Flat Fault Mine)



PMD-22
(Heart's Desire Mine)

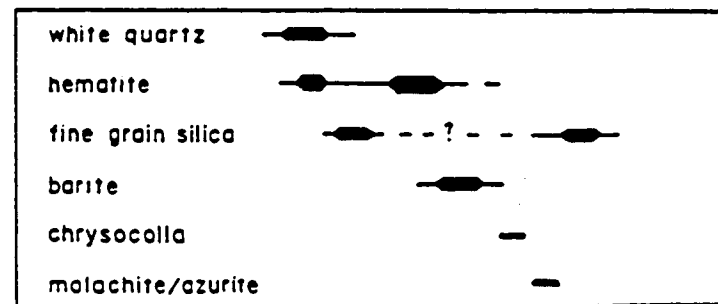


Figure 14- continued

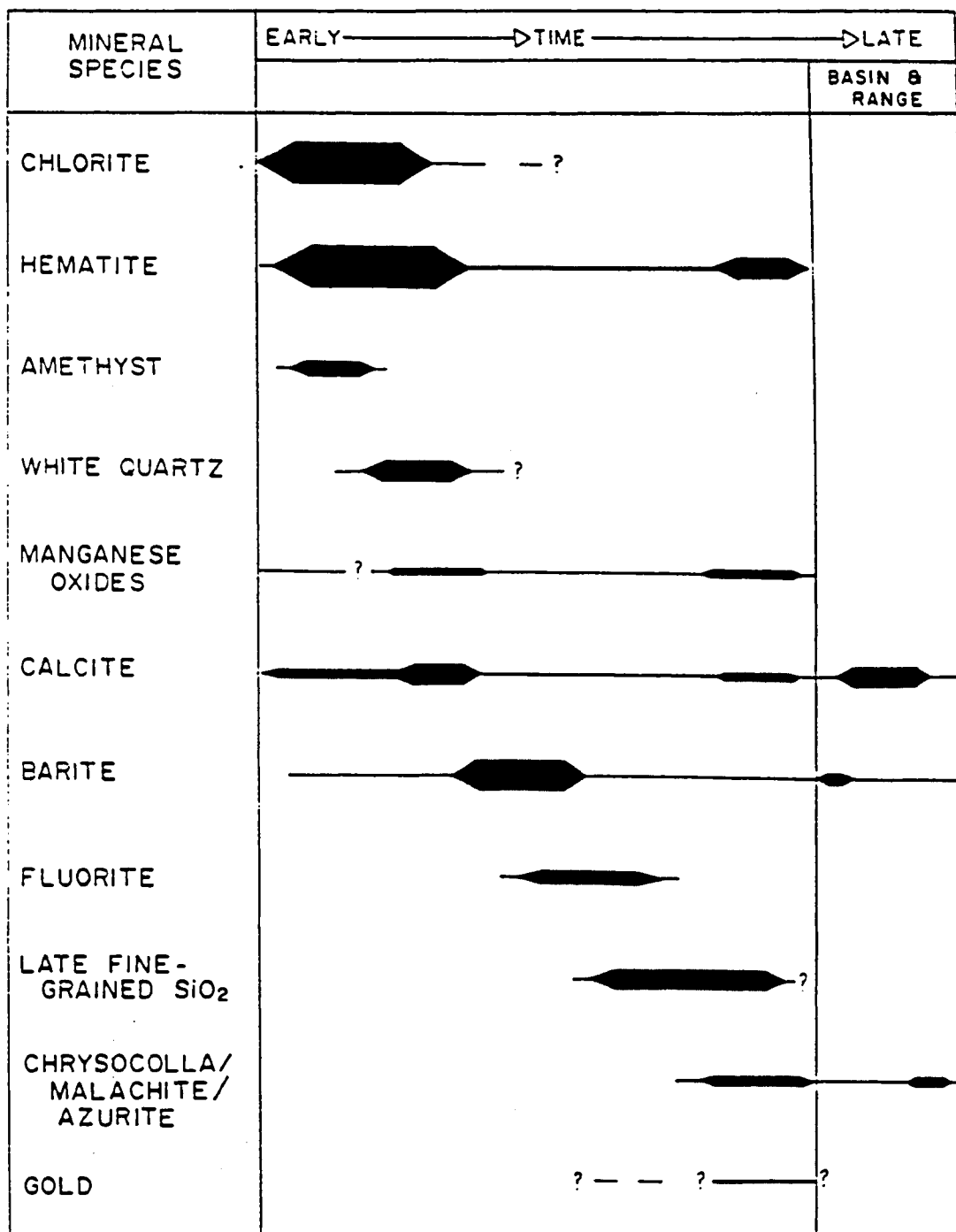


Figure 15- Generalized paragenetic sequence for the Northern Plomosa district.

mineralization is widespread chloritic alteration (see plate 2). This style of alteration is most pronounced and most widespread in the silty, red to orange, calcareous sediments, usually near mineralized fault veins. It is well developed around the Little Butte mine and in the west half of section 7, around several smaller mines and prospects. The chloritic alteration imparts a distinctive dark green color to the originally orange to brown sediments. In thin section, the chlorite is variably pleochroic from green to light green, yellow-green or brown-green. It is in textural equilibrium with blady specular hematite. The assemblage also includes minor calcite and sparse elongate euhedral quartz grains which are clearly not detrital in origin.

Chloritic alteration also affected the Proterozoic crystalline rocks. Chlorite has replaced biotite in the granitoid rocks. In one instance near the Arrastre mine in section 8 a mafic dike that intrudes the Proterozoic granite is largely replaced by an assemblage of chlorite and specular hematite. Pyroxene in phenocrysts and in the ground mass is replaced by chlorite and specularite. There is evidence of sequential replacement, with chlorite followed by hematite; however, in many cases bladed hematite exists in apparent equilibrium with interstitial well-crystallized chlorite (see Figure 16).



Figure 16- Photomicrograph of hematite/chlorite assemblage in textural equilibrium replacing pyroxene phenocryst in mafic dike near Arrastre Mine. Plane polarized light; field of view is approximately 0.4mm wide.

2. Specular hematite replacements

The second stage in the paragenetic sequence within the calcareous rocks of the limestone-tuff unit is represented by massive specular-hematite replacements of limestone. These hematite replacement bodies are the most visually striking hydrothermal features in the area; they are particularly well developed in the eastern half of section 7, within the area of strong chloritic alteration. While hematite of this stage is again locally in textural equilibrium with less abundant chlorite, the majority of the hematite is later than the chloritic alteration. Evidence of fracture control is abundant, but replacement textures around the fractures indicate that replacement accounts for most of the specular hematite present in the rocks. The most complete replacement is of the gray limestone layers, which are in places converted to 85-90% hematite by volume. Minor chlorite and calcite are also part of the replacement assemblage. In some cases minor amounts of manganese oxides are intermixed with the hematite, or cut it in veinlets. The hematite replacement has also affected unchloritized rocks to a lesser extent.

Open-space Filling Mineralization

1. Early quartz-hematite stage

In the volcanic unit and especially the Plomosa conglomerate, the early stage of chlorite and hematite replacement is much less significant than it is in the

calcareous sediments; an early open-space-filling quartz-hematite phase occurred instead. Earliest in this sequence are crustified cockscomb amethyst and earthy hematite which fill narrow (5-20 cm) fault veins in Plomosa conglomerate. Contemporaneous mineralization and fault movement are evident from the brecciation of crustified vein-filling material and the development of a matrix which includes earthy and specular hematite and less prominent unbrecciated amethyst. Microscopic study of the amethyst reveals a "feathery" texture and incomplete extinction indicative of recrystallization from chalcedony. Quartz with these characteristics makes up over half of the amethyst in the sections examined petrographically. In these sections the clear, coarsely crystalline amethyst is interrupted by hematite-rich crusts consisting of microcrystalline quartz and flakes of specular hematite, as well as by crusts of opaque earthy hematite. Locally the amethyst veins are cored by white quartz which displays less evidence of recrystallization from chalcedony.

The amethyst veins do not include any of the later stages of the paragenetic sequence. However, white quartz that is in every observable way similar to that coring the amethyst veins forms the earliest stage of mineralization in several prospects developed within the Plomosa conglomerate, including the Scotchman mine. The Scotchman mine is developed on a fault vein which places Plomosa conglomerate against the

volcanic unit in the southeast corner of section 12. The vein contains abundant white, euhedral, open-space filling quartz (up to 2 cm) with relatively minor hematite-rich crusts. The early quartz and hematite are followed by the later paragenetic stages described below.

2. Late barite, fluorite, silica, and oxidized copper

Following the chlorite and hematite alteration stages in the calcareous sediments and the early quartz-hematite stage in the Plomosa conglomerate, a well established sequence of barite, fluorite, and oxide copper mineralization occurred. Euhedral white barite and later colorless to sea-green fluorite encrust earlier-stage minerals. A fine-grained silica phase consisting of chalcedony and/or fine-grained (less than 1 mm) euhedral quartz is generally contemporaneous with and later than the fluorite. This phase is present in growth zones within fluorite and replacing barite, as well as in veinlets cutting both barite and fluorite. Still later chrysocolla, malachite and azurite cut earlier phases. This latest assemblage is present in veinlets and as a breccia matrix along with earthy hematite.

3. Latest, supergene, and unrelated(?) mineralization

Minor manganese oxides are scattered through the established paragenetic sequence and are most commonly associated with hematite. Veins containing predominantly manganese oxides, with or without calcite and barite, are only

common in the volcanic unit, and cross-cutting relationships are not abundant. Manganese oxides and calcite do cut barite, suggesting that they form a late stage, but their place in the overall sequence is not clear.

Late colorless to orange calcite that cuts or encrusts all stages of the recognized paragenetic sequence could be supergene in origin, as could some of the late oxidized copper minerals.

Postdetachment high-angle faults in the area host minor mineral deposits which are distinct from and probably unrelated to the important mineralization in the district. These deposits take the form of narrow (10-30 cm) veins with filling consisting of minor early barite and a main stage of coarse dark brown, crustiform calcite. The dark brown color of the calcite is imparted by abundant hematite inclusions and minor acicular clusters of manganese oxides. One of these veins cutting the lower plate metamorphic rocks in the south half of section 24 contains fine-grained euhedral quartz, chrysocolla, and a narrow (2-3 cm) zone of iron oxide gossan after sulfides at the core of the vein.

Evidence of hydrothermal sulfide mineralization was observed in this study only in the lower plate of the Plomosa detachment fault. One example is the vein just described. Other minor occurrences of iron oxide and copper staining in the lower plate possibly reflect sulfide mineralization, but

could not be related to the upper-plate paragenetic sequence.

Jemmett (1966) attributed iron staining in the Proterozoic crystalline rock near the Little Butte open pit to oxidized sulfides, and reported that disseminated pyrite was encountered in drill holes at depths below 100 meters in that area. On the basis of the lack of any sulfide mineralization in the Tertiary section, he suggested that the pyrite was older than the Tertiary rocks in the district.

The only other distinctive style of mineralization in the district is exemplified by the mine just north of the road in the southwest quarter of section 18 which is identified by Jemmett (1966) as the Granite mine. A rather deep shaft is developed in unfoliated Proterozoic granitic rock; examination of the dump reveals that the target was white bull quartz indistinguishable from that which is common as lenses and pods throughout the Proterozoic rocks of the area. Local residents claim that the mine was a significant gold producer. The size of the workings, the lack of any significant iron or copper staining, and the significant precious metals values (see Chapter 6) in the dump material lend credence to the claim that gold was the primary target. No obvious controlling structure is exposed at the surface.

Economic mineralization

The important economic mineralization in the district is consistently associated with the latest stages of the

paragenetic sequence. Bancroft (1911) described the ores of the Little Butte mine as "a breccia of chrysocolla and malachite cemented by specularite." Jemmett (1966) described the ores of several of the more recently developed mines in similar terms, but noted that the oxidized copper minerals are commonly also part of the breccia matrix. He also observed gold to be late in the sequence, occupying microfractures in the earthy-hematite matrix to breccia in the Dutchman mine. This author's inspection of the larger workings in the area generally confirm the observations of the previous investigators, but red-brown earthy hematite is apparently more common as a late stage breccia matrix than specularite. No gold was observed, but production figures indicate that these ores contained significant gold as well as the obvious copper mineralization. Assays of dump material taken during the course of this study confirm that the highest values, both in copper and gold, are associated with the brecciated earthy hematite vein material containing abundant chrysocolla, malachite, and fine grained silica.

Host rock associations

While the paragenetic sequence described above is consistent throughout the district, in no one occurrence can all the stages be observed in the proportions indicated on Figure 15. As indicated in the description of the sequence, there is a strong association of certain styles of

hydrothermal mineralization with specific rock types or units. The pervasive chloritic alteration is associated primarily with the orange calcareous sediments, and locally affects the ferromagnesian minerals in the Proterozoic basement and mafic volcanic rocks. The massive specular-hematite replacements formed preferentially within the thicker limestone layers in the same unit. Fracture-controlled manganese oxide mineralization is only common in the Tertiary volcanic unit. Large crustified quartz veins are seen only within or in contact with the Plomosa conglomerate, and the amethyst-hematite veins only in a small area of Plomosa conglomerate on the northwest flank of Beehive hill.

Small barite-hematite veinlets (less than 0.5 cm wide) are widespread across the mapped area, but almost all of the significant barite mineralization is within or in contact with the volcanic unit. Large barite(±fluorite ±quartz ±calcite ±hematite ±manganese oxide) occurrences are common within the volcanic unit and in the immediately overlying Plomosa conglomerate; and have been observed only rarely elsewhere in the geologic column.

In the case of the chlorite and hematite replacements, the association is almost certainly host-rock control attributable to the reactive nature of the calcareous sediments; but in the other cases the host-rock associations are less readily explained.

Structural controls on Mineralization

With the exception of the replacement chlorite and hematite, which exhibit marked stratigraphic control, most of the hydrothermal mineralization within the Northern Plomosa district is localized by high-angle faults. Measured fault veins dip from nearly horizontal in the case of the Flat Fault deposit to nearly vertical. Strikes of mineralized faults and veins fall predominantly within the northwest compass quadrant (Figure 17). Relatively few mineralized faults strike northeast, although northeast-striking faults are not uncommon in the area.

There is relatively little evidence for significant control of mineralization by low-angle faults in the area. The hematite bodies replacing limestone blocks in the Tertiary carbonate section seem to be associated with minor bedding plane slip, but they are also associated with widespread and pervasive alteration near major high-angle faults. The influence of host rock seems the more important factor localizing these replacement bodies. Round Mountain is itself a thrust block, and is intensely thrustured internally, but no noticeable control has been exerted by any of these low-angle faults upon the sparse mineralization in the block.

The one very important low angle fault that is notable for its lack of mineralization is the detachment fault. Over the limited length of its outcrop in the mapped area, the

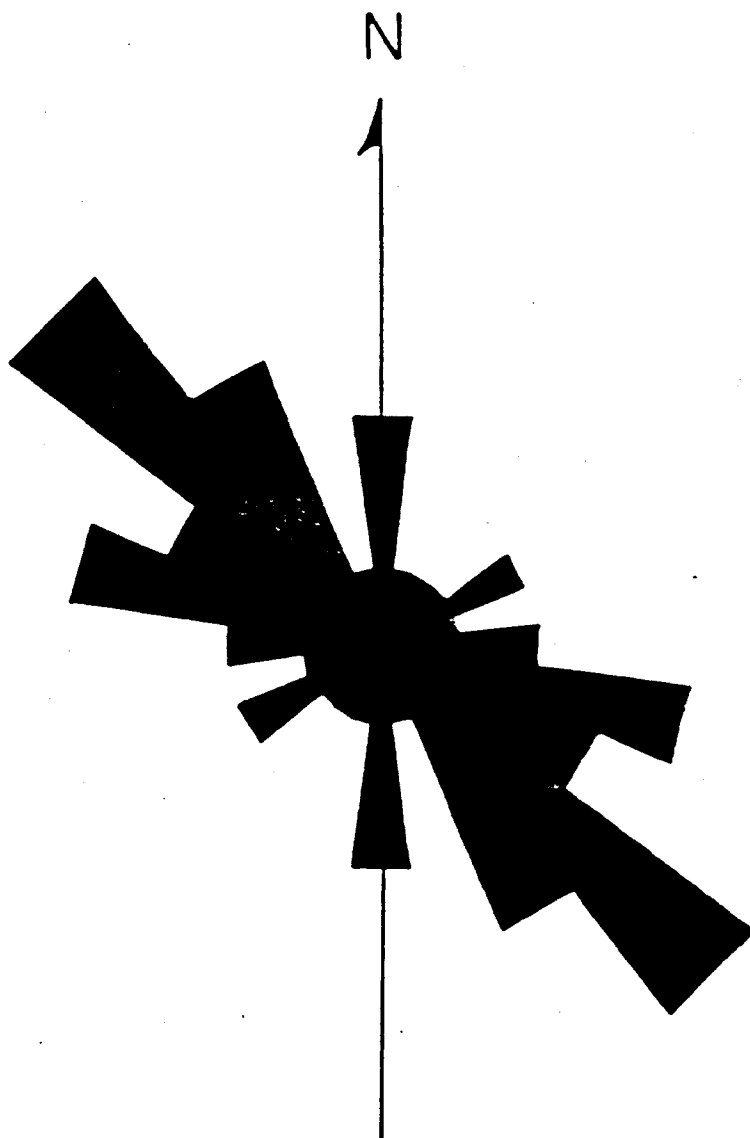


Figure 17- Rose diagram: strikes of 29 mineralized faults in the Northern Plomosa district.

fault zone itself shows no sign that it ever acted as a conduit for hydrothermal fluids. The crushed zone is loose and friable; it is neither silicified nor argillized, nor otherwise altered to any degree. Copper staining is notably absent in the fault zone, although minor copper mineralization, unaccompanied by the other stages of the recognized upper plate assemblage, is present at shallow levels in the lower plate. Hydrothermal mineralization immediately adjacent to the detachment fault is limited to thin (less than 2 cm), discontinuous barite stringers in the lower plate chloritic rocks a few meters from the fault zone, and this barite is distinctive isotopically from other barite in the district (see Chapter 7).

High angle north-striking postdetachment faults host minor calcite-barite-quartz-sulfide mineralization described earlier.

CHAPTER 5

Fluid inclusions

Thirteen samples of likely gangue material were collected from dumps and outcrops in the Plomosa district for fluid inclusion study. These samples were prepared as doubly polished thick (100-200 mm) sections and studied petrographically to supplement mesoscopic observations of mineralization before they were destroyed in the course of fluid-inclusion work. Of the thirteen samples prepared, nine were found to contain fluid inclusions amenable to study, but only seven contained primary fluid inclusions.

All fluid-inclusion work was performed by the author in the fluid-inclusion laboratory of The University of Arizona. The system used was manufactured by S.G.E., Inc. of Tucson, Arizona, using a modified U.S.G.S. design. The system was calibrated using synthetic fluid inclusions obtained from Synflinc, Inc. at Penn State University. Heating measurements reported here are considered to be accurate to within $\pm 1.0^{\circ}\text{C}$, and cooling temperatures are accurate to $\pm 0.3^{\circ}\text{C}$.

In all, 490 temperature measurements were recorded from

a total of 273 fluid inclusions. The temperature at which the fluid inclusion contents homogenize to one phase upon heating (T_h) and the temperature at which the inclusion contents melt upon warming after freezing ($T_m(\text{ice})$) were recorded from primary fluid inclusions contained in minerals representing four different stages in the paragenetic sequence. These stages are: 1) early amethyst, 2) white cockscomb quartz, 3) fluorite, and 4) late fine-grained quartz. Homogenization and melting temperatures were gathered from secondary inclusions in all of the above mentioned stages as well. Figures 18 and 19 present all heating and freezing data in the form of histograms. No primary fluid inclusions were positively identified in barite, therefore all data from that phase are considered to be from secondary inclusions. Eutectic first melting temperatures were very difficult to ascertain, because of both the limited optical capabilities of the system and the subtle nature of the early stages of the phase change itself. Where the appearance of liquid was observed, the temperature measurement is probably a maximum estimate of the eutectic temperature.

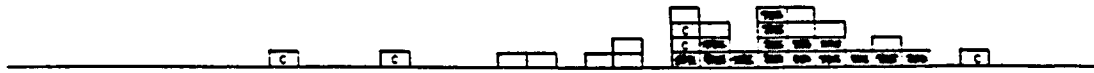
Primary Fluid inclusions

1. Amethyst

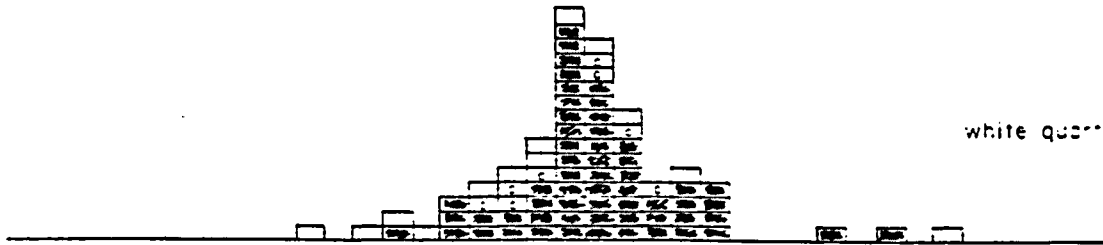
Amethystine quartz from the western flanks of Beehive Hill in the west half of section 13 (see plate 2) is the earliest stage in the paragenetic sequence to yield fluid-

□ secondary
▨ andesitic (primary)
▩ primary

amethyst



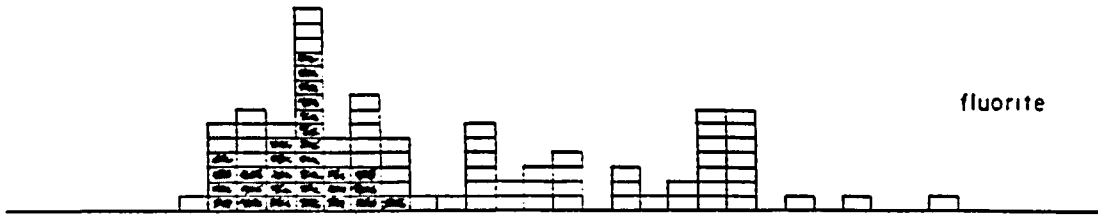
white quartz



barite



fluorite



late fine qtz.

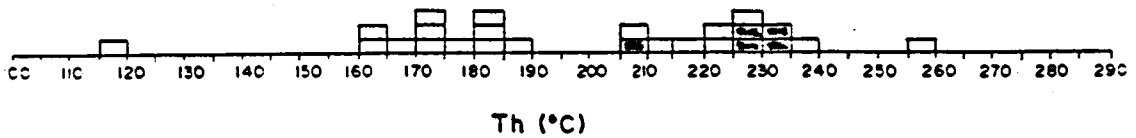


Figure 18- Histogram showing homogenization temperatures (Th) of all primary and secondary fluid inclusions.

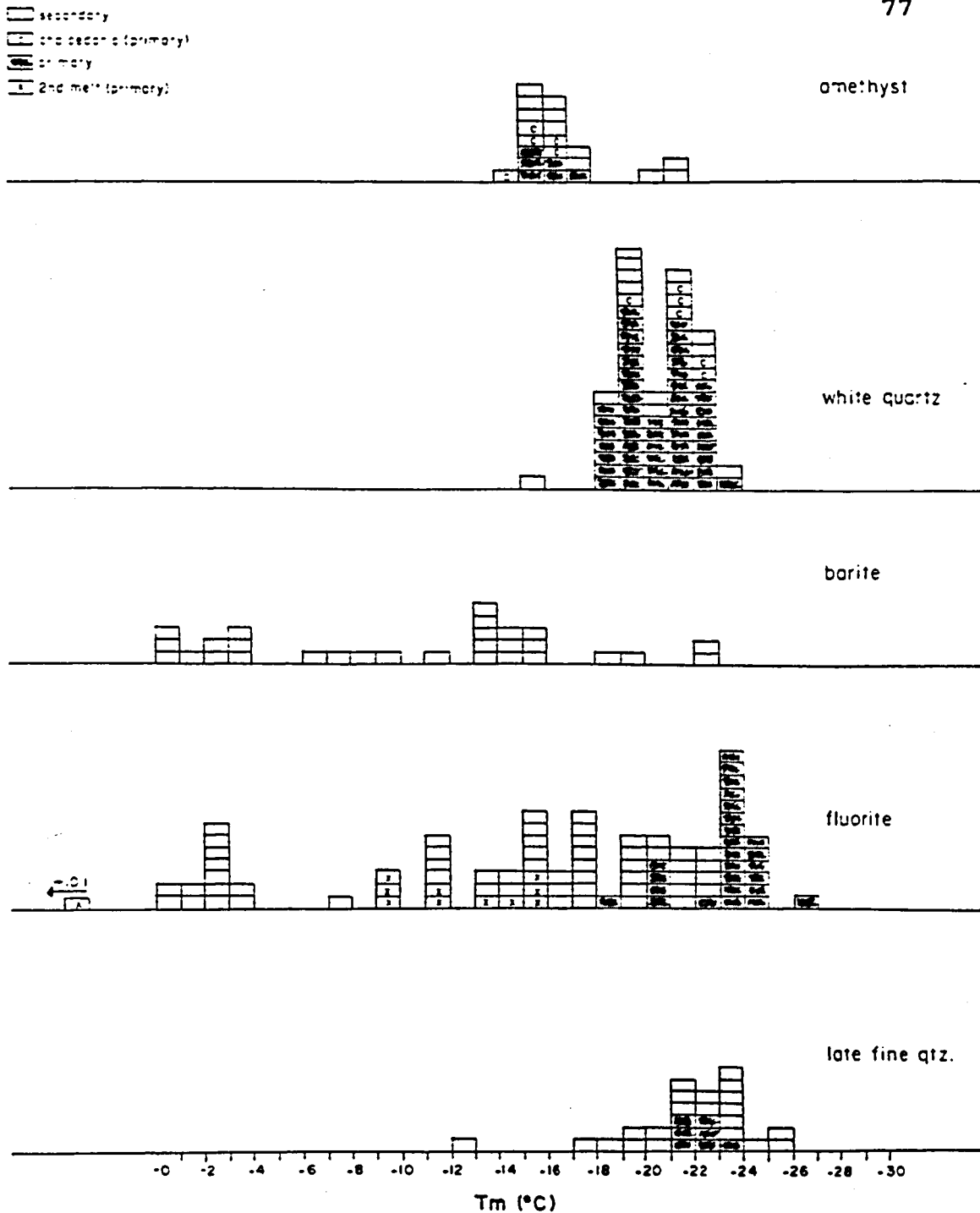


Figure 19- Melting temperatures (T_m(ice)) for all primary and secondary fluid inclusions. Also shown are the temperatures of the second (higher temperature) melting event observed in several primary inclusions in fluorite.

inclusion data. In general, the amethyst is remarkably free of fluid inclusions; in two polished sections, only one narrow (less than 1 mm) growth zone was found to contain usable primary inclusions. The primary inclusions that did yield data are small (5-15 μ) and concentrated on phantom pyramid faces of the amethyst crystals. The inclusions are of two phases, liquid and gas, with gas apparently occupying 10-20% of the cavity volume. Temperatures from primary fluid inclusions in both primary quartz and recrystallized chalcedony were recorded.

Homogenization temperatures for non-chalcedonic amethyst cluster around a mode between 230 and 235°C. Homogenization temperatures for inclusions in recrystallized chalcedony are not as well grouped, and tend to skew the mean for the whole population to a lower temperature. The amethyst represents the highest temperature group of fluid inclusions studied here.

$T_m(\text{ice})$ from primary fluid inclusions in amethyst range from -14.9 to -17.4°C and form a mode between -15 and -16°C. If the fluid was a simple solution of NaCl and water these melting temperatures would represent a range of salinity from 18.7 to 20.7 wt. % salt. These estimates represent the lowest salinities of any primary inclusions observed in this study. Eutectic temperatures recorded fall in the range of -30 to -35°C.

2. White quartz

Primary inclusions in the white quartz are abundant in growth zones which involve both recrystallized chalcedony and primary crystalline quartz (Figure 20). The inclusions are growth lineated with long dimension up to 50μ and gas bubbles occupying about 10 - 20% of total volume (Figure 21). Homogenization temperatures for primary crystalline white quartz form a well defined mode near 200°C , and range from 178°C to 255°C . Homogenization temperatures from inclusions in recrystallized chalcedony do not differ significantly.

The range of $T_m(\text{ice})$ data from primary fluid inclusions in white quartz is from -18.8 to -23.2°C . The data are bimodal with peaks between -19 and -20°C and between -21 and -22°C . The T_m modes would represent salinities of approximately 22.5 and 23.5 wt. % NaCl, respectively, if NaCl was the only salt present in solution. However, because the eutectic for a water-NaCl solid-ice solution falls at -21.8°C , any simple NaCl-water solution in which the final melting temperature for ice is below -21.8°C should also contain crystalline NaCl. No NaCl solid phase was observed in any fluid inclusion in this study, therefore it is apparent that other solutes exist in significant amounts in the fluids in question and figures given for equivalent weight percent NaCl are relevant only for purposes of comparison. Eutectic temperatures for the white quartz phase are slightly lower

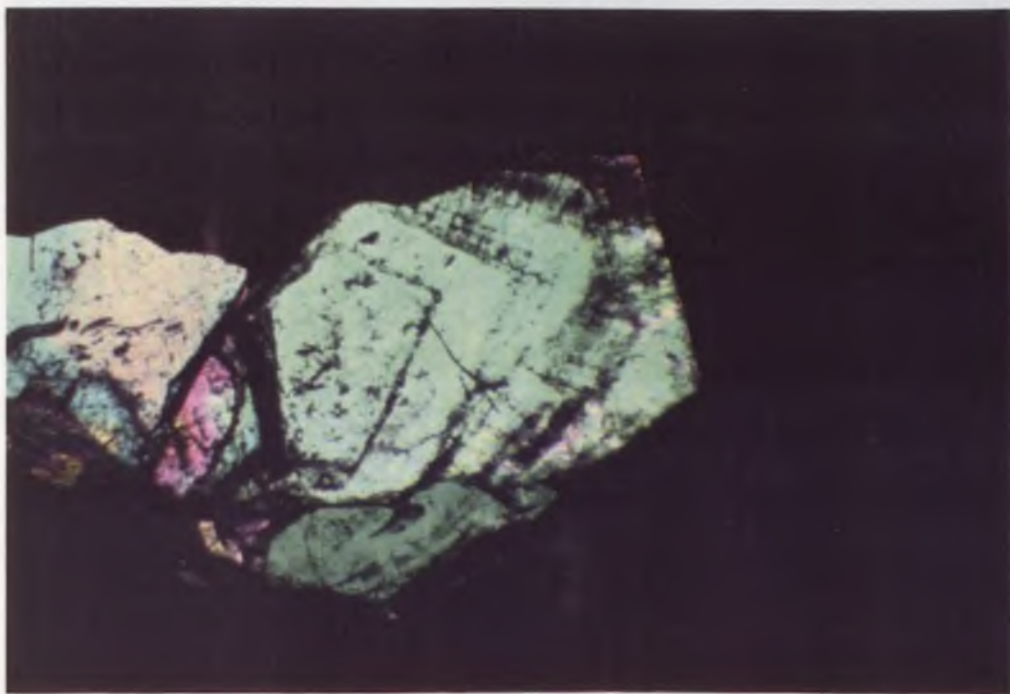


Figure 20- Growth zone in white quartz showing fluid inclusions concentrated along growth planes and the variably chalcidonic textures observable in a single crystal. Specimen from the Scotchman mine (PMD-28). Field of view is approximately 6.2mm wide; crossed polars (thick section).

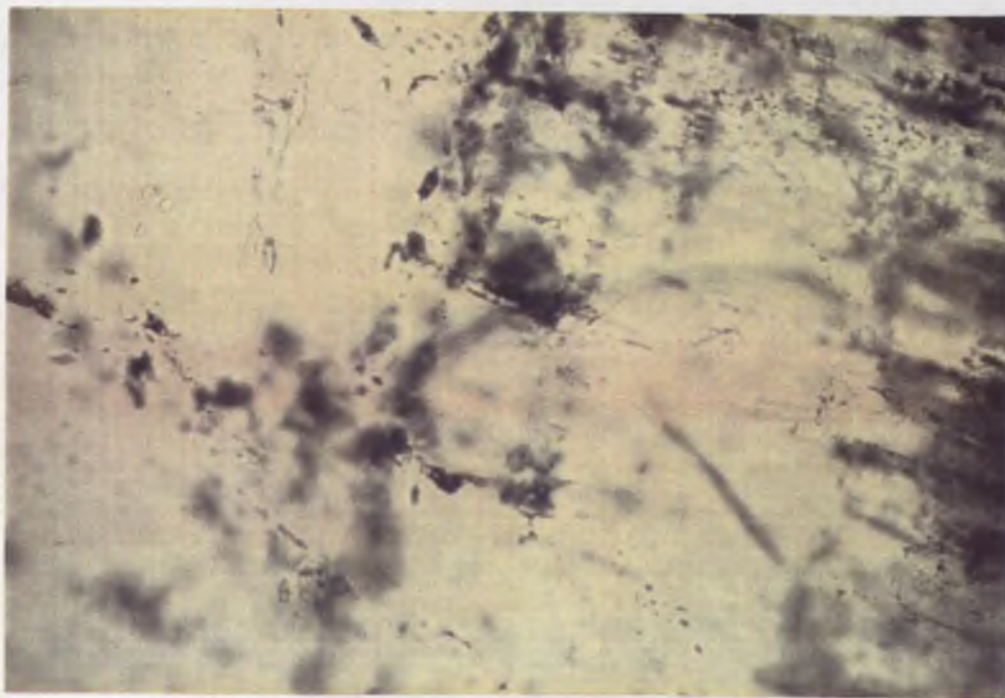


Figure 21- Fluid inclusions in white quartz from the Scotchman mine (PMD-28). Primary inclusions are growth lined and concentrated in growth zones. Plane polarized light; field of view is approximately 0.4mm wide.

than those for amethyst, falling in general near -35°C .

3. Fluorite

Homogenization temperatures from primary inclusions in fluorite form a single well defined mode between 150 and 155°C , with a range from 136°C to 163°C , and as a group constitute the lowest temperatures of any stage studied here. Most of the data in this group are from a single fluorite crystal from a large barite-fluorite occurrence contained within Tertiary volcanic rocks in the east half of section 17 (sample PMD-15). In this crystal, growth lineated inclusions are developed perpendicular to a growth zone defined by inclusions of euhedral microcrystalline quartz. Eight of the data points, including the distinct group of higher melting temperatures in Figure 19, are from the Scotchman vein (sample PMD-28). One primary inclusion in fluorite was identified in material from the dump of the Adele M. mine in the Northwest corner of section 18 (sample PMD-7). All of the primary inclusions in fluorite showed low gas-to-liquid ratios consistent with their low homogenization temperatures. Final melting temperatures for primary fluid inclusions in fluorite are also the lowest of any encountered in this work, ranging from -18.8 to -26.3°C with a mode between -23 and -24°C . A secondary mode between -20 and -21°C is again attributable to the influence of the data from sample PMD-28. Eutectic temperatures for primary fluid inclusions in fluorite range

from -35 to -45°C, with most near -40°C.

The low values of $T_m(\text{ice})$ for primary inclusions in fluorite further reinforce the inference that NaCl is not the only solute present in the fluid. Minimum eutectic temperatures of less than -45°C are also not consistent with a pure NaCl system. In addition, an unexplained melting phenomenon is observed in ten of the growth-lineated fluid inclusions from sample PMD-15 and the one from sample PMD-7. In each of these inclusions two distinct and repeatable melting events were observed. The lower-temperature event falls consistently at or near the T_m mode for all primary inclusions in fluorite, and involves the greater proportion of the solid material in the partially frozen fluid inclusion. This event displays all the characteristics of a normal final melting of water-rich ice, and is interpreted here to be exactly that. In these few inclusions, however, the final melt of water-rich ice leaves a second solid in equilibrium with the fluid. This solid is yellow, and of higher relief than the ice. The second solid is of variable abundance in the inclusions at T_m , and its final melting temperature increases with its abundance. The final melting temperatures of the second solid range from -16.0°C to +10.1°C, with all but one between -16.0 and -9.3°C.

4. Late fine-grained quartz

The latest paragenetic stage from which fluid-inclusion

data were obtained is composed of fine-grained (<1mm) quartz and microcrystalline silica. Owing to the small size of the crystals, only a few usable primary fluid inclusions were found in this stage. The mode for this group is defined by only four data points and falls between 225 and 235°C, with one Th outside that range at 206°C. The seven melting temperatures obtained range only from -21.5 to -23.1°C, forming a broad mode between -21 and -23°C. Eutectic temperatures fall in the range from -40 to -45°C.

Secondary Fluid Inclusions

Homogenization and melting temperatures were measured and recorded from a total of 154 secondary fluid inclusions representing all stages from which primary data was collected. The early quartz stages contain relatively few secondary inclusions, and the few measurements made fell within the ranges defined by the data from the primary fluid inclusions for both the amethyst and the white quartz.

The barite studied contains abundant fluid inclusions, not all of which are clearly secondary, but because no primary inclusions were definitely identified all the data are considered to be from secondary inclusions for the purposes of this study. Figure 19 shows that melting temperatures for fluid inclusions in barite ranged from -0.3°C to -22.8°C with no dominant modal value. In general, homogenization temperatures for fluid inclusions in barite were not reliable.

Repeated heating of a single inclusion most often resulted in no consistent T_h value. The five T_h measurements that were considered reliable fall within the range 211°C to 237°C.

Measurements of T_h recorded for secondary inclusions in fluorite range from 132°C to 261°C; T_m varies from -0.6 to -23.0°C. Neither the T_h nor the T_m data cluster around any dominant modal value, but figures 18 and 19 suggest at least four secondary modal groupings. Eutectic temperatures for secondary fluid inclusions in fluorite span the range from -30 to -45°C.

A total of 23 secondary fluid inclusions in the late fine grained quartz indicate a range for T_h from 119°C to 256°C, and for T_m from -12.0 to -25.4°C. The eutectic temperatures cluster between -40 and -45°C.

Interpretation of Fluid Inclusion Data

Figure 22 is a T_h versus $T_m(\text{ice})$ plot of all primary fluid inclusions that highlights the distinct fluids from which the different phases were deposited. All fluid-inclusion data presented here are raw numbers. No attempt has been made to correct for pressure in the homogenization data or to equate freezing temperatures with NaCl solute concentrations. The field evidence indicates that the hydrothermal minerals were deposited at shallow but unknown depths which probably did not exceed 2 km in the deepest cases and perhaps a few hundred meters in the highest level veins

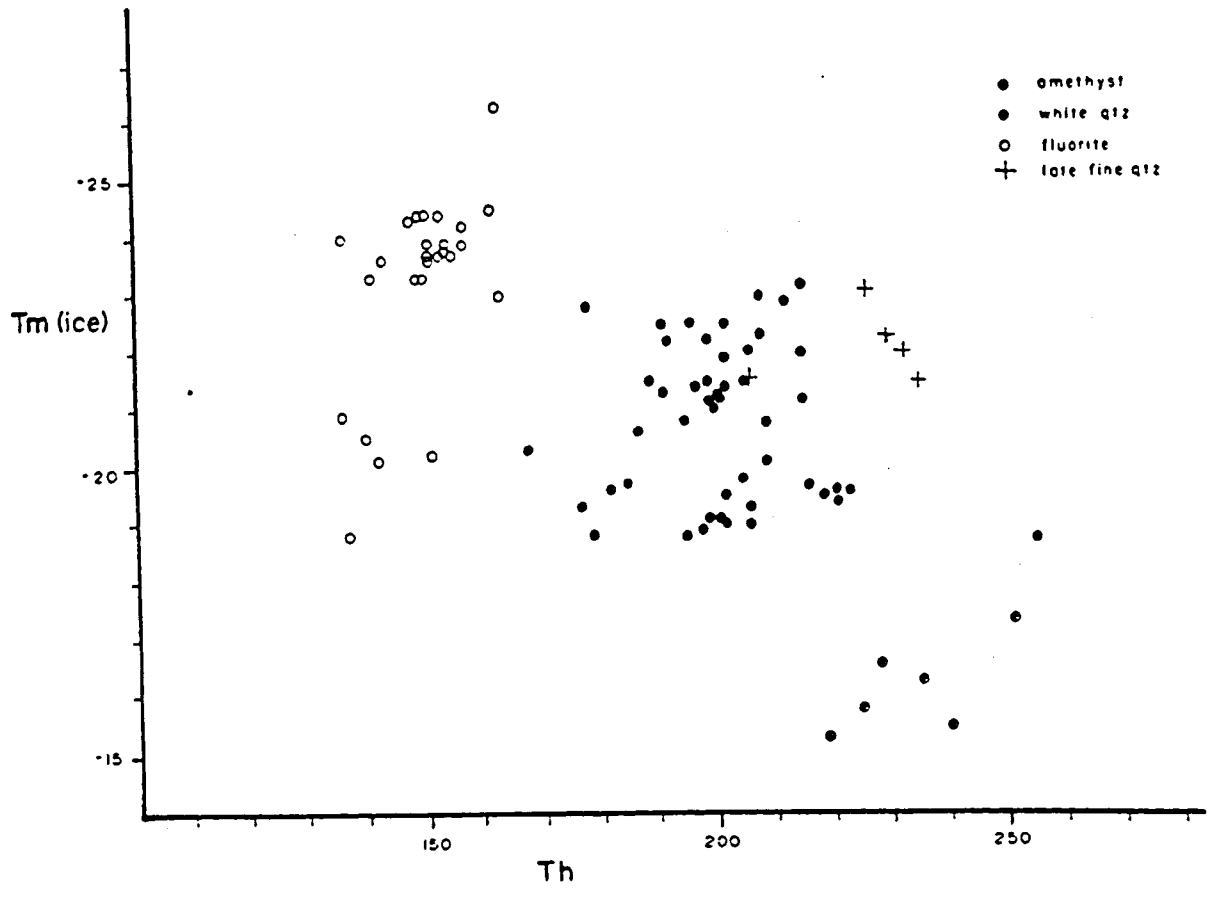


Figure 22- Plot of Th vs. Tm(ice) of primary fluid inclusions for which both values could be obtained.

in the Plomosa conglomerate. Potter's (1977) curves indicate that pressure corrections necessary to estimate minimum filling temperatures would increase T_h values by less than 20°C if hydrostatic conditions are assumed for a maximum depth of 2km. Referring to NaCl equivalent salinities would be misleading, as the lack of daughter NaCl crystals combined with the low values of $T_m(\text{ice})$ indicates clearly that solutes other than NaCl were part of the system.

The unexplained melting phenomenon described earlier for some primary inclusions in fluorite, and the low eutectic temperatures further support the inference that unidentified solutes are present. The identification of these solutes is not possible without analytical work which is beyond the scope of this study, but calcium and sulfate ions were certainly present in the hydrothermal system in some, possibly significant, concentration. The work of Crawford et al. (1979) indicates only calcium chloride solutions are known to have eutectic temperatures below -35°C. Whatever the exact solution composition might have been, the fluids can be confidently identified as moderately concentrated brines, probably with NaCl as the dominant solute.

Any further interpretation of the fluid inclusion data must first acknowledge the limits of the data when taken as representative of the entire district and of the whole paragenetic sequence. Table 2 lists the sources of fluid-

	PMD-30	PMD-28	PMD-17	PMD-3	PMD-8	PMD-4	PMD-9
Amethyst	20 / 11						
White qtz.		67 / 14					
Borite			0 / 10	0 / 19			
Fluorite		8 / 13	20 / 0	0 / 17	0 / 27	1 / 16	
Late fine qtz.						7 / 13	0 / 10

Table 2- Sources of fluid inclusion data presented in this study. For mineral phase and locality, the number of primary fluid inclusions from which data was obtained is above the slash and the number of secondary inclusions below.

inclusion data. A total of six thick sections representing only five localities yielded all of the primary data. No paragenetic stage is represented by primary data from more than three localities, and no locality provided primary data on more than two phases.

Accepting the limitations of the fluid-inclusion data, an interesting pattern is evident when it is combined with paragenetic relationships. Primary fluid-inclusion data for the amethyst, white quartz, and fluorite develop a consistent picture of a hydrothermal system in which early higher temperature and lower salinity fluids become cooler and more saline with time. The late fine-grained quartz, however, seems to reverse the earlier trends. While the data set from this latest stage of primary fluid inclusions is small, it is sufficiently distinctive to indicate with some confidence that the hydrothermal system was rejuvenated with fluids of higher temperature and slightly lower salinity at a late stage in its evolution. This inference is supported by the abundant relatively high temperature and lower salinity secondary inclusions in barite and fluorite.

A large number of secondary fluid inclusions in fluorite were studied, both because their size and abundance made data acquisition easy and because they offered the chance to confirm the evidence from primary fluid inclusions in the late-stage fine-grained quartz that the later fluids did not

continue the cooling and concentrating trend established in the earlier stages. These data clearly indicate that most later fluids were hotter and less saline than those from which the fluorite was deposited (see figures 18 and 19). In some cases the fluids were hotter and less saline than those which deposited the late fine-grained quartz, suggesting the possibility that the system continued its rejuvenation beyond the period recorded by primary fluid inclusion data.

Previous fluid inclusion studies (Allen, 1985; Wilkins et al., 1986, 1988; Bradley, 1987; Spencer et al., 1988; Roddy et al., 1988) have associated certain fluid characteristics with detachment fault-related mineralization. Most fluid inclusions from detachment-related deposits contain only two phases, liquid and vapor, although Allen (1985) found CO₂-rich inclusions and Wilkins et al. (1986) reported some hydrocarbons. No studies have revealed evidence of boiling. Homogenization temperatures range generally from low (<150°C) to moderate (approximately 325°C), and fluid salinities are consistently moderate to high (12 to 25 wt. % NaCl eq.). Wilkins et al., (1986) found on the basis of a broad sampling of detachment-related deposits that homogenization temperatures were higher on average in quartz than in fluorite and calcite, but found no correlation between salinity and temperature or mineral species. Homogenization and melting temperatures found in Northern Plomosa district minerals place

the district within the temperature range defined by Wilkins et al. (1986) for detachment related deposits, and at the high end or slightly above the normal range of salinity for such deposits (see Figure 23).

Overall, the fluid inclusion evidence, as well as the mineralogical evidence, strongly supports the classification of the Northern Plomosa district among detachment-related deposits. No previous work, however, has revealed the detailed relationships between temperature, salinity and time (or paragenetic stage) found in the Northern Plomosa district mineralization.

Roddy et al., (1988) found relatively high temperatures (270-330°C) in and near the Bullard detachment fault, and lower temperatures away from the fault. Bradley (1987) reported consistently low homogenization temperatures (120-180°C) in barite, calcite, fluorite, and quartz from the Silver district in southern La Paz County, Arizona. The Silver district is considered to be detachment-related, but because the detachment fault is not exposed in the district, it is interpreted to be high in the upper plate and distal from the fault. As in the Silver district, the mineral assemblage and generally low homogenization temperatures in the Northern Plomosa district suggest a position high in the upper plate. Projection of the Plomosa fault beneath the district supports this interpretation; most of the known

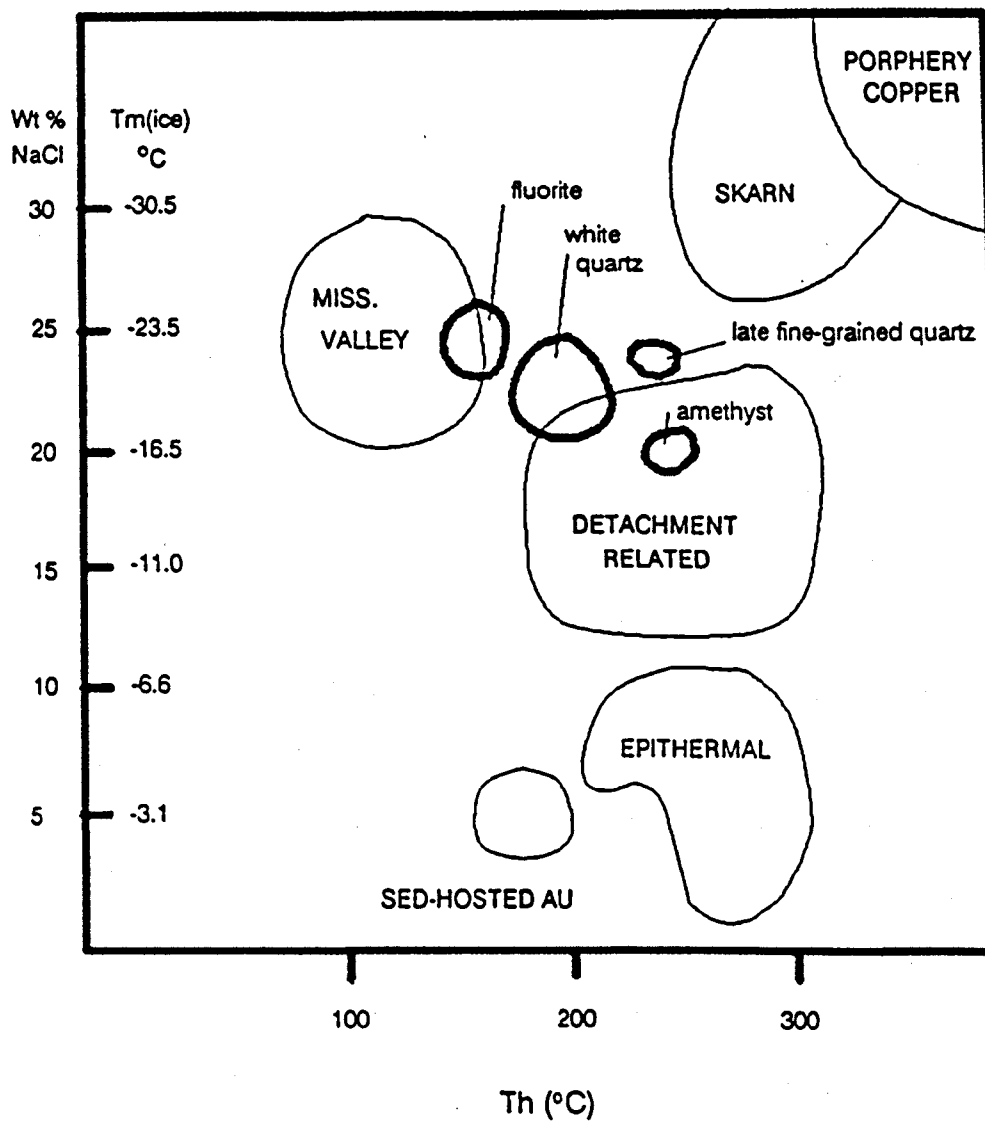


Figure 23- Plot of salinity vs. homogenization temperature for several classes of mineral deposit (dashed outlines); after Wilkins et al., (1986). Salinities were determined by measurement of melting temperatures and are thereby comparable to Northern Plomosa district mineralization (solid outlines).

deposits are probably more than 500 meters above the detachment.

Several workers (Wilkins and Heidrick, 1982; Beane et al., 1986; Spencer and Welty 1986; 1989; Wilkins et al., 1986; Roddy et al., 1988) have suggested models for detachment-related mineralization in which heat from the lower plate or tectonic deformation induces saline basin waters to flow upward along regional, low-angle detachment faults and into permeable upper plate rocks. The uniformly high fluid inclusion salinities found in the Northern Plomosa district, combined with the local K-metasomatism and inferred extensional basin environment, support the interpretation that evaporative basin brines were the basic fluid involved in the hydrothermal system. The variation in fluid temperature and salinity through the paragenetic history of the Northern Plomosa system, however, requires the addition of a degree of complexity to the earlier models. One suggested refinement calls on hot, deep brines moving upward and mixing with cooler waters near the surface (Spencer and Welty, 1989). If this hypothesis is applied to the Northern Plomosa district, the correlation of lower temperatures with higher salinities suggests that the surface waters were more saline than the deep, upwelling brines.

The rejuvenation of fluid conditions inferred for the late stages of the Northern Plomosa system is also not

explained by the existing simple models. The temperature variations could be explained by varying rates of flow of the hot, deep fluids brought about by episodic extension and permeability changes related to faulting. Alternatively, while no likely candidate was uncovered in the course of this study, an igneous source of heat and fluids is not out of the question.

Another question to be addressed is the relevance of the fluid-inclusion data to the economic mineralization in the district. None of the early paragenetic stages is consistently associated with gold or copper, which are the only significant ore metals. From the descriptions of the occurrence of visible gold (Bancroft, 1911; Jemmett, 1966) and the strong correlation of gold with visible copper mineralization (see Chapter 6), it is evident that the gold was deposited late in the evolution of the mineralizing system. A possible correlation also exists between gold and a late, fine-grained silica phase, present in abundance in the two samples that yielded the highest gold analyses in this study. Thus, whereas no direct evidence links gold (or copper) to the late, fine-grained quartz stage from which fluid-inclusion data was obtained, that stage is considered the most likely of any to have some relationship to economic mineralization.

With this connection in mind, it is interesting to note

that homogenization temperatures in the late, fine quartz are significantly (70°C) higher than in the previous and/or contemporaneous fluorite stage, but salinities (as inferred from melting temperatures) are only slightly lower. The possibility that a late, relatively high temperature and high salinity fluid might have the greatest capacity to transport metals in a system such as the one that apparently operated in the Northern Plomosa district is discussed in Chapter 8.

CHAPTER 6Exploration Geochemistry

Thirty samples from across the Northern Plomosa district were collected for geochemical analysis for metal content. The population consists of 23 samples which are composed dominantly of hydrothermal minerals collected from dumps and mineralized outcrops, and 7 samples of country rock altered to varying degrees. Although the sample population is small, an attempt was made to provide a fair representation of the larger workings and of the different styles of mineralization and alteration in the district, and to achieve a reasonably even coverage of the mapped area. The samples were analyzed by atomic absorption spectrophotometry at Skyline Labs in Tucson, Arizona, for Au, Ag, As, Mo, Cu, Pb, Zn, and Te. A listing of sample numbers with descriptions is provided in appendix (A). Table 3 is a listing of the raw data from the analyses.

The small number of data make contouring of metal values a very subjective exercise, but in general high gold values and high copper values concentrate in a northeast trending

EXPLORATION GEOCHEMISTRY

97

SAMPLE #	Au	Ag	As	Mo	Cu	Pb	Zn	Te
PMD 1	<0.05	0.05	0.8	2	85	2	4	<0.1
PMD 2	<0.05	0.25	3.2	<2	110	16	18	<0.1
PMD 3	<0.05	0.05	8	4	3050	8	6	<0.1
PMD 4	<0.05	<0.05	3	<2	930	12	22	<0.1
PMD 5	<0.05	<0.05	65	<2	650	20	12	<0.1
PMD 6	<0.05	<0.05	15	8	5050	8	8	<0.1
PMD 7	<0.05	0.1	26	6	27000	12	12	0.4
PMD 8	<0.05	<0.05	155	35	1500	32	12	<0.1
PMD 9	10	0.05	22	4	36000	22	12	<0.1
PMD 10	6.4	0.1	48	8	47000	16	38	0.2
PMD 11	<0.05	<0.05	2.6	18	12500	18	12	<0.1
PMD 12	<0.05	2.6	9	2	250	48	16	<0.1
PMD 13	<0.05	0.15	90	30	100	50	18	<0.1
PMD 14	2.1	1.1	22	4	2550	18	28	0.2
PMD 15	<0.05	0.05	25	<2	630	16	26	<0.1
PMD 16	1.6	1.5	1.8	<2	1400	18	190	25
PMD 17	<0.05	<0.05	19	<2	24	36	185	<0.1
PMD 18	<0.05	0.25	6.5	<2	25000	1450	2650	0.2
PMD 19	0.15	0.75	0.2	<2	13000	25	12	0.1
PMD 20	0.15	0.45	6.5	<2	340	16	38	3
PMD 21	<0.05	<0.05	0.8	<2	440	8	16	<0.1
PMD 22	9.5	0.1	11	<2	37000	32	14	0.3
PMD 23	<0.05	<0.05	165	<2	60	12	26	<0.1
PMD 24	0.55	<0.05	30	4	1250	14	10	<0.1
PMD 25	<0.05	<0.05	24	18	120	18	55	0.2
PMD 26	<0.05	0.05	3.6	6	26	20	44	<0.1
PMD 27	<0.05	0.2	26	8	16	32	8	<0.1
PMD 28	0.1	<0.05	2.2	<2	445	4	4	<0.1
PMD 29	<0.05	<0.05	1.4	<2	16	30	90	<0.1
PMD 30	0.05	0.05	1.8	<2	55	4	4	0.1

Table 3- Raw geochemical data from 30 dumps and outcrops in the Northern Plomosa district. All values are in parts per million. See Plate 2 For sample locations.

band stretching from the Heart's Desire (Plomosa) mine in the southwest to the Little Butte mine in the northeast. The highest arsenic values apparently flank the Au-Cu band to the northwest and southwest (refer to plate 2). The highest silver values (still economically insignificant) are concentrated in the southern half of the mapped area. Lead and zinc exist in significant concentrations only in sample PMD-18 which is from the vein, described earlier, controlled by a postdetachment high-angle fault; this mineralization is quite distinct from and probably unrelated to the main body of mineralization in the district. Tellurium is important only in sample PMD-16 which consists of bull quartz from Proterozoic granite, again a style of mineralization distinct from most of that in the area. Molybdenum is not present in significant quantities in any of the samples analyzed.

Correlation coefficients between the metals were calculated for the raw data and are presented in Table 4. The strong positive correlation between copper and gold ($r=+0.78$) is the most obviously significant. Correlations between gold and silver and between gold and arsenic are notable by their absence; both show insignificantly small negative correlation coefficients. Arsenic does correlate positively (+0.553) with molybdenum. Tellurium is the only element besides copper to have a positive correlation with gold; this correlation is very weak. The calculated

CORRELATION COEFFICIENTS

	Au	Ag	As	Mo	Cu	Pb	Zn	Te
Au	1	-0.039	-0.035	-0.1	0.785	-0.066	-0.074	0.037
Ag		1	-0.171	-0.173	-0.132	0.007	0.01	0.422
As			1	0.553	-0.053	-0.072	-0.093	-0.124
Mo				1	-0.05	-0.078	-0.108	-0.107
Cu					1	0.256	0.241	-0.085
Pb						1	0.995	-0.037
Zn							1	0.027
Te								1

Table 4- Correlation coefficients between the eight metals analyzed for in geochemical sampling of Northern Plomosa district mineralization.

correlation coefficient between lead and zinc is very strongly positive; however, this number is misleading. If sample PMD-18 (the high Pb-Zn sample) is deleted from the population, the correlation coefficient for lead and zinc is only +0.229. Correlation coefficients of similar magnitude exist between the other base metals (excluding molybdenum) and between silver and the base metals.

Ratio Analysis

As might be expected from a sampling of this sort, values for the individual metals vary by as much as three orders of magnitude between samples, and average concentrations of the different metals vary by almost as much. For these reasons, the geochemical data were treated using a ratio analysis based on that developed by Roger Newell (1974) in his dissertation on the Tombstone district. The process involves multiplying the values for each of the metals by a specific factor, thereby adjusting the average value of each of the species to approximately the same order of magnitude and affording each an equal weight in the ratio formula. Using the adjusted data, the ratio is produced by dividing the value for the metal in question by the sum of the remaining metal values. Because of the great range of values resulting from this method, and because of the tendency of data sets such as this one to be lognormally distributed (Davis, 1986, p.87), the ratios are transformed to log₁₀ values to produce the final

"ratio values" used here. The formula used to produce the ratio values and the specific adjustment factors used for the metals are given in Figure 24. For the purposes of this calculation, and for the calculation of correlation coefficients, analyses below detection were averaged in at the detection limit for the element in question.

The intent of this effort is to gain some understanding of the hydrothermal mineralization in the district. For this reason samples that are not composed dominantly of hydrothermal minerals, and are therefore likely to reflect host-rock chemistry rather than hydrothermal chemistry, are not suitable for ratio analysis. Samples PMD- 13, 20, 23, 25, 26, 27, and 29 are composed of variably altered "country rock" of various types, and were deleted from the data set for the purposes of the ratio analysis, leaving a set of 23 samples. The final ratio values of the 23 samples are provided in Table 5.

"High" ratio values were determined subjectively by designating a cutoff value at a natural break in the data distribution above which a reasonable fraction (in this case, 14-33%) of the values lie. Outlining high ratio values as they are distributed on the map of the district (plate 2) produces several notable groupings. Northeast-trending bands of high gold- and copper-ratio values stretching in general from the area of the Little Butte mine in the northeast to the

ADJUSTMENT FACTORS:

Au x 10,000

Cu x 1

Ag x 100,000

Pb x 1000

As x 1000

Zn x 1000

Mo x 10,000

Te x 10,000

FORMULA FOR CALCULATING RATIO VALUES:

$$\text{RATIO VALUE} = \log_{10} \left[\frac{\text{element in question x its adjustment factor}}{\text{sum of: [each other element x its adjustment factor]}} \right]$$

Figure 24- Adjustment factors and formula for calculating "ratio values" in table 5 and on plate 2.

RATIO VALUES

SAMPLE #	Au	Ag	As	Mo	Cu	Pb	Zn	Te
PMD 1	5.18	6.25	5.39	7.17	4.41	5.8	6.13	5.49
PMD 2	4.78	6.63	5.6	6.5	4.12	6.37	6.44	5.08
PMD 3	4.85	5.88	6.1	7.1	5.65	6.1	5.96	5.15
PMD 4	4.89	5.92	5.69	6.65	5.17	6.36	6.71	5.2
PMD 5	4.61	5.62	7.04	6.28	4.74	6.28	6.03	4.91
PMD 6	4.61	5.63	6.14	7.27	5.63	5.84	5.84	4.92
PMD 7	4.52	5.85	6.32	6.82	6.34	5.93	5.93	5.43
PMD 8	3.95	4.95	6.58	7.24	4.42	5.78	5.33	4.25
PMD 9	6.88	5.33	6.01	6.31	6.25	6.01	5.73	4.63
PMD 10	6.42	5.53	6.27	6.55	6.26	5.74	6.15	4.82
PMD 11	4.33	5.34	5.09	7.54	5.76	5.93	5.74	4.64
PMD 12	4.15	7.44	5.42	5.78	3.85	6.19	5.67	4.45
PMD 13	4.02	5.51	6.37	7.24	3.32	6.07	5.6	4.32
PMD 14	5.97	6.92	6	6.29	5.02	5.9	6.11	4.92
PMD 15	4.71	5.73	6.61	6.41	4.81	6.29	6.55	5.02
PMD 16	5.4	6.48	4.45	5.5	4.34	5.46	6.62	6.8
PMD 17	4.27	5.28	5.89	5.91	2.95	6.19	7.36	4.58
PMD 18	3.08	4.78	4.31	4.68	4.78	6.73	7.24	3.68
PMD 19	5.01	7.01	4.13	6.19	5.98	6.31	5.95	4.83
PMD 20	4.98	6.6	5.63	6.16	4.34	6.05	6.5	6.37
PMD 21	4.99	6.03	5.2	6.8	4.93	6.26	6.65	5.29
PMD 22	6.87	5.67	5.72	6	6.3	6.23	5.83	5.14
PMD 23	4.34	5.35	7.41	5.98	3.54	5.74	6.11	4.64
PMD 24	5.73	5.69	6.59	6.78	5.07	6.18	6.01	4.98
PMD 25	4.25	5.25	5.98	7.24	3.63	5.83	6.38	4.85
PMD 26	4.57	5.59	5.44	6.91	3.29	6.24	6.69	4.88
PMD 27	4.48	6.13	6.26	6.96	2.98	6.37	5.7	4.78
PMD 28	5.44	6.19	5.79	7.05	5.08	6.08	6.08	5.44
PMD 29	4.53	5.54	4.98	6.19	3.03	6.41	7.19	4.83
PMD 30	5.14	6.2	5.72	7.09	4.18	6.09	6.09	5.45

Table 5- "Ratio Values" calculated for 23 samples of hydrothermal mineralization from dumps and outcrops in the Northern Plomosa district. Areas of "high" values of Au, Ag, As, and Cu are shown on Plate 2.

Heart's Desire (Plomosa) mine in the southwest show almost complete overlap and highlight the correlation between those metals. No high Cu-ratio values, and only one high Au ratio on the south side of Round mountain, falls outside the outlined zones. These bands also encompass most of the significant mines of the district. High arsenic-ratio values are nowhere coincident with high gold or copper values and seem, on the basis of relatively few data points, to define zones on the northwest and east edges of the district, marginal to the central Cu-Au zone. High silver-ratio values do not show any significant correlation with gold, copper or arsenic, and form a separate zone which trends NW-SE in the southern part of the district and overlaps the Cu-Au zone only on the northern flanks of Beehive hill.

The ratio values paint effectively the same picture as the raw data and the correlation calculations. In fact, a number of variations of the ratio formula were tried, for example using \log_{10} values and deleting metals which are apparently unimportant in the hydrothermal system. In each case the result was essentially the same.

The important facts brought out in this analysis include the strong positive correlation between gold and copper, and the relatively insignificant correlations between gold and other metals, or between any other metals. Some zoning of metals can be inferred, most notably in the form of a copper-

gold center and a high arsenic periphery. The NE-SW trend of these zones is interesting as it does not lend itself easily to any interpretation linking the hydrothermal system directly to the northwest-striking Plomosa detachment fault. The high silver zone in the southern part of the district shows no clear relationship to the Au-Cu-As trend. It is in general closer to the Plomosa fault than the high copper-gold and high arsenic zones, but to suggest a zoning of silver, gold, and arsenic at progressively greater distance from the detachment fault does not seem justified.

CHAPTER 7Stable Isotope Geochemistry

In the attempt to further characterize the fluids which were responsible for mineralization in the Northern Plomosa district, and for deposition of the chemical sediments in the area, a total of 46 determinations of stable isotopic character were performed on a total of 31 samples. Eleven $\delta^{34}\text{S}$ and five $\delta^{18}\text{O}$ values were obtained from eleven samples of hydrothermal barite from across the district; and $\delta^{13}\text{C}$ and $\delta^{18}\text{O}$ values were obtained from a total of ten samples of hydrothermal and sedimentary carbonates. Carbonate minerals analyzed include one sample of malachite, five varieties of hydrothermal calcite, and 4 different sedimentary carbonate rocks from the district. All stable isotope determinations were done in the laboratory of stable isotope geochemistry at the University of Arizona. Most of the analyses were performed by Dr. Christopher J. Eastoe and the author; two oxygen determinations on barite were done by James R. Lang. All stable-isotope values obtained as part of this study are presented in Table 6.

STABLE ISOTOPE DATA

107

sample #	description	del 34 S (CDT)	del 18 O (SMOW)	del 13 C (PDB)
BARITE:				
PF 1	lower plate stringer	+6.4 per mil	+8.2 per mil	
PF2	lower plate stringer	+7.2 per mil		
PMD-1	big barite vein	+11.3 per mil		
PMD-11	Flat Fault Mine	+12.3 per mil	+10.7 per mil	
PMD-3	Beehive Hill vein	+16.3 per mil	+12.2 per mil	
PMD-8	Airstrip deposit	+11.6 per mil		
PMD-28	Scotchman Mine	+14.4 per mil	+10.5 per mil	
PMD-26	red Tertiary LS w/ba	+11.4 per mil		
PMD-15	ba/fl prospect	+16.9 per mil	+13.2 per mil	
PMD-10	Little Butte Mine	+11.4 per mil		
PMD-21	ba veins	+12.6 per mil		
CARBONATE SEDIMENTS:				
PMD-27	brown Tertiary LS		+18.1 per mil	-1.7 per mil
PMD26	red Tertiary LS		+19.3 per mil	-0.8 per mil
2-18-3	gray PZ LS/DOL		+19.6 per mil	-0.4 per mil
PMD-29	pC/PZ LS/DOL sliver		+18.2 per mil	-3.0 per mil
HYDROTHERMAL CARBONATES:				
PMD-17	orange ca in pCg		+21.9 per mil	-3.1 per mil
PMD-15	brown altration ca		+26.6 per mil	+0.6 per mil
PMD-3	late ca in BHH vein		+18.3 per mil	-2.3 per mil
10-88-1	late ca in qtz vein		+25.0 per mil	-5.4 per mil
PMD26	ca vein in Red Tert. LS		+23.5 per mil	-1.4 per mil
PMD-22	malachite		+23.2 per mil	-5.9 per mil

Table 6- All stable isotope values generated by this study.

Sulfates

Hydrothermal barite was collected from nine mines and prospects representing a relatively even coverage of the mineralized district, and from two small stringers from the lower plate of the detachment near its outcrop in the northwest corner of section 19. $\delta^{34}\text{S}$ values were determined for all the barite samples, and $\delta^{18}\text{O}$ values were determined for five of those samples representing the full range of $\delta^{34}\text{S}$ values.

Sulfur dioxide for sulfur isotope analysis was prepared from barite samples by combustion at 1100°C with Cu_2O and SiO_2 , using the methods of Coleman and Moore (1978). For oxygen isotope analysis, CO_2 was prepared by heating barite with graphite under high vacuum conditions. All CO evolved was converted to CO_2 , and all CO_2 was collected by cooling with liquid nitrogen. Gas samples were analyzed on a VG602C double collector mass spectrometer. Repeated analyses of lab standards have resulted in analytical precision of $\pm 0.3\text{‰}$ (2σ) for $\delta^{34}\text{S}$, and $\pm 0.8\text{‰}$ for $\delta^{18}\text{O}$.

Figure 25 is a histogram showing the distribution of $\delta^{34}\text{S}$ values for barite and the relationship of that distribution to the district stratigraphy. $\delta^{34}\text{S}$ values range from +6.4 to +16.9‰ and reveal a rough correlation exists between position in the stratigraphy and barite $\delta^{34}\text{S}$ value. The two highest $\delta^{34}\text{S}$ values represent samples from Plomosa

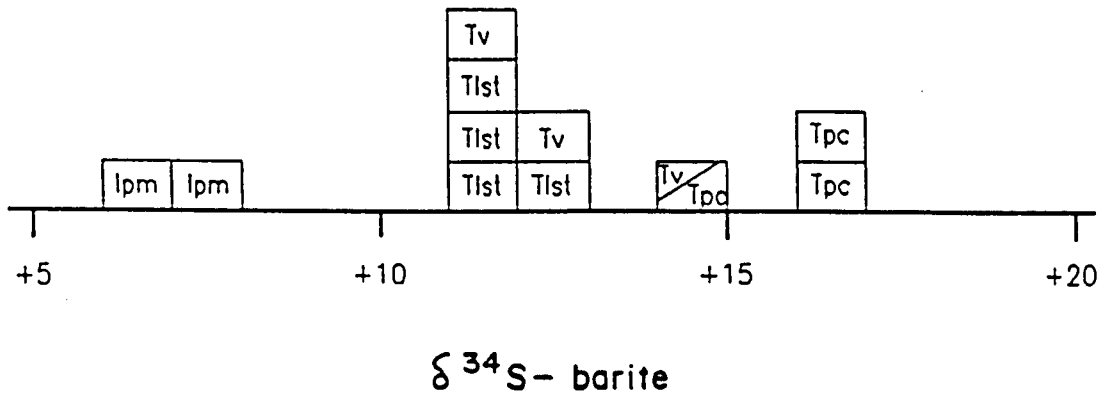


Figure 25- Histogram of $\delta^{34}\text{S}$ values in Northern Plomosa district barite. Symbols indicate the map units which host the barite samples; two symbols separated by a slash indicates that the barite was hosted by a fault which juxtaposed the two units.

conglomerate, the highest stratigraphic unit. The cluster of values between +11.3 to +12.6‰ are all from barites hosted by Tertiary units (T1st and Tv) from the middle of the Tertiary stratigraphic sequence, and the intermediate-value (+14.4‰ $\delta^{34}\text{S}$) barite is from the Scotchman mine, which is developed on a fault that places Plomosa conglomerate against the Tertiary Volcanic unit. The two lower-plate barites have the lowest $\delta^{34}\text{S}$ values at +6.4 and +7.2‰.

Oxygen isotopic values for barite range from +8.2 to +13.2‰. Figure 26 is a plot of $\delta^{18}\text{O}$ versus $\delta^{34}\text{S}$ values for barite in the district. Despite the low precision of the $\delta^{18}\text{O}$ values, a correlation between $\delta^{18}\text{O}$ and $\delta^{34}\text{S}$ is evident.

Also plotted on Figure 26 is the Quiburis gypsum, a middle Tertiary lacustrine evaporitic gypsum from the San Pedro Valley near Mammoth, Arizona. The $\delta^{34}\text{S}$ value of the Quiburis gypsum was established C. J. Eastoe and the $\delta^{18}\text{O}$ value by James R. Lang, both in the Laboratory of Isotope Geochemistry at the University of Arizona. The dashed outline represents the range of $\delta^{18}\text{O}$ and $\delta^{34}\text{S}$ values obtained from sulfate precipitated from ground water samples from several basins in southeast Arizona (Kalin, unpublished data). All of these data show correlations between $\delta^{18}\text{O}$ and $\delta^{34}\text{S}$ similar to that in the Northern Plomosa district barite. The cause of the evident correlation between sulfur and oxygen isotopes in both the ground waters and the Northern Plomosa

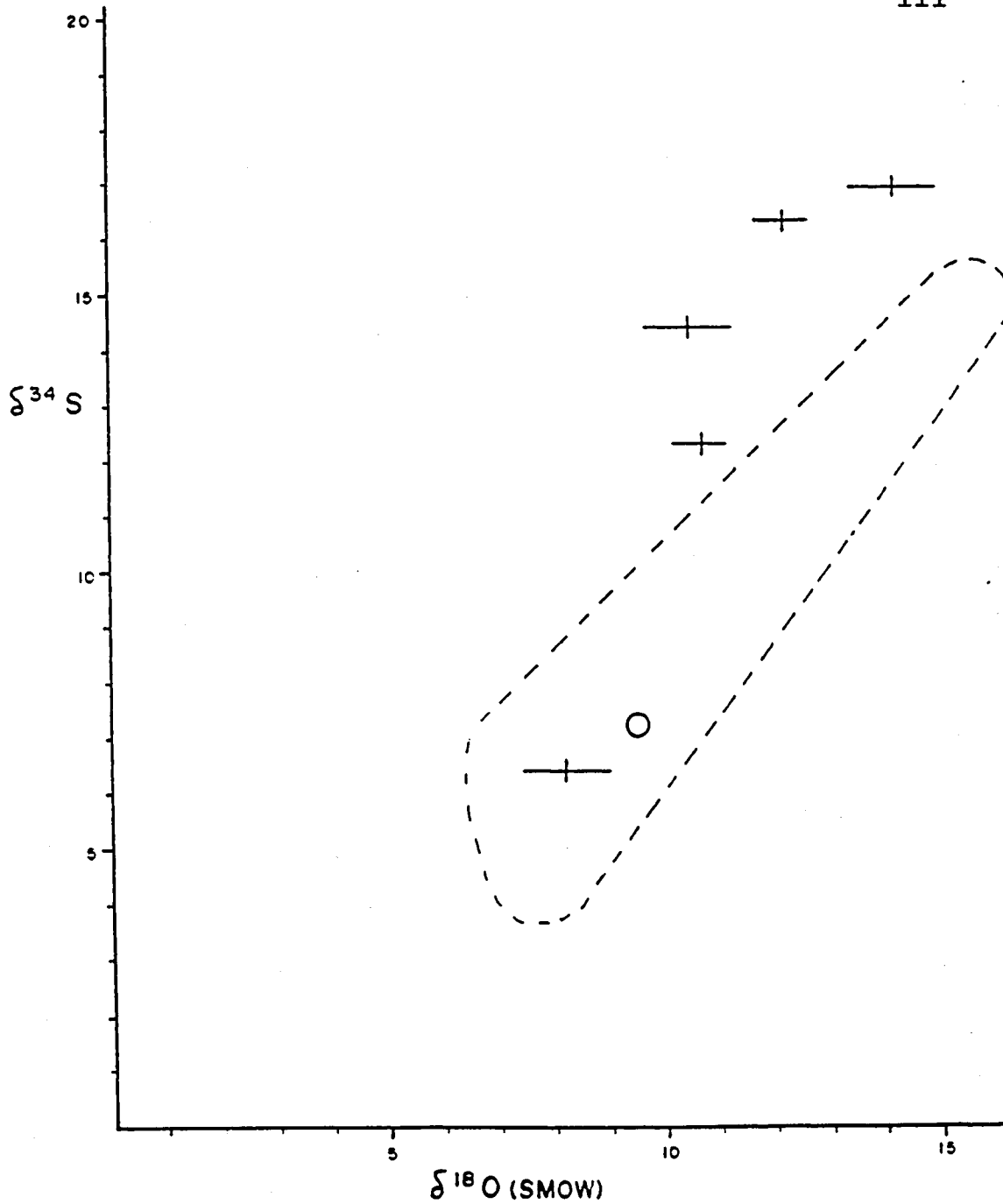


Figure 26- Plot of $\delta^{18}\text{O}$ vs. $\delta^{34}\text{S}$ in Northern Plomosa district barite. Vertical and horizontal error bars reflect the accuracy of values generated as part of this study. The open circle represents the Quiburis Gypsum, and the dashed outline represents sulfate precipitated from modern ground waters from basins in southeastern Arizona (Kalin, unpublished data).

district barites is not clear. The trend suggests at least two sources of sulfate, one containing heavy sulfur and oxygen (at least $+15\text{‰}$), and another containing lighter sulfur and oxygen (less than $+7\text{‰}$).

Permian to Triassic marine evaporites are known to have $\delta^{34}\text{S}$ and $\delta^{18}\text{O}$ values in the range of $+12$ to $+17\text{‰}$ and $+11$ to $+15\text{‰}$ respectively (Claypool et al. 1980), and to crop out in both southeastern Arizona and in the Plomosa Mountains south of the study area. Claypool et al. (1980) also suggested that sulfate produced by the oxidation of pyrite in the weathering environment should contain oxygen of $\delta^{18}\text{O}$ of about $+2\text{‰}$, owing to fractionation of heavy ($+23\text{‰}$) atmospheric oxygen and incorporation of lighter (-10‰) oxygen from meteoric water (Lloyd, 1968). Sulfides would be expected to contribute relatively light sulfur, as well. Pyritic shales are abundant in the lower part of the Paleozoic section in southeast Arizona, as are sulfides associated with porphyry copper deposits. Neither of these were observed in the immediate vicinity of the Northern Plomosa district, but Jemmett (1966) did report disseminated pyrite in the Proterozoic rocks, and most normal igneous rocks also contain some sulfur.

The two distinct sources of sulfate discussed represent possible end members of a mixing trend. At surface temperatures it is unlikely that any significant isotopic equilibration occurs between the oxygen in the water and that

in the dissolved sulfate (Claypool et al., 1980). Therefore, the sulfate $\delta^{18}\text{O}$ values (as well as the $\delta^{34}\text{S}$ values) in basin waters probably reflect the values of the sulfate contributed from erosional or other sources. For the southeastern Arizona basins, surface waters could have contributed both sulfate end members, or surface waters could have contributed lighter sulfate derived from weathering of sulfides, and deep-circulating geothermal waters which probably exist in the basins (Stone, 1989) could have added heavy sulfate from Paleozoic evaporites.

The strong similarities between the isotopic characteristics of the Northern Plomosa district barites and the southeastern Arizona ground waters suggests that similar sources of sulfur are involved. However the data suggest some complications to any simple mixing hypothesis. The consistent paragenetic relationships indicate that most of the upper plate barite was probably deposited at nearly the same time and conditions within the hydrothermal system, but it is possible, depending on the amount of post-mineralization displacement on the Plomosa fault, that lower plate barite is unrelated. Deletion of the lower plate data would weaken the apparent mixing trend seen in Figure 26. Also, even considering the uncertain relevance of the lower plate barite, the correlation between sulfate isotopic character and position within the stratigraphy suggests that some

stratigraphic or host-rock control played a part in any sulfate-mixing mechanism. This suggestion of stratigraphic or host-rock control is strengthened by the observation that volumetrically significant barite deposits are restricted to the upper Tertiary (Tv and Tpc) units in the district.

Some amount of isotopic equilibration between sulfate oxygen and fluid oxygen would normally be expected during involvement in a hydrothermal system and would tend to muddy the picture further. Although no direct fluid inclusion evidence is available as to the temperature of deposition of the barite analyzed, a reasonable guess would place it between those of fluorite (approximately 160°C) and white quartz (approximately 200°C). The work of Chiba and Sakai (1985) indicates that at 200°C and near neutral pH, oxygen isotopic equilibration between sulfate and water would probably take over ten years. At 150°C, equilibration would require closer to 10^5 years. These numbers indicate that any equilibration of sulfate with water in the system probably did not closely approach completion. Therefore, no reliable estimates of fluid $\delta^{18}\text{O}$ value can be made here, and hydrothermal barite $\delta^{18}\text{O}$ values probably still reflect to some degree the isotopic compositions of the sulfates originally contributed to the brines from the inferred erosional (and other?) sources. Because no hydrothermal sulfides were observed in the district, no questions of sulfide-sulfate equilibration are

considered here. It is assumed that barite $\delta^{34}\text{S}$ values also reflect the values of contributed sulfate.

One possible explanation for the observed correlations in sulfate isotopic data is that the connate basin brines were compositionally stratified. Erosional sources of sulfate that changed with time could have resulted in brines containing lighter sulfate concentrated in the lower parts of the section, and heavier sulfates upward. Sulfate derived from the oxidation of the Tertiary volcanic rocks (by K-metasomatizing fluids?) could also have contributed to the stratification of sulfate isotopic compositions.

Another possibility is that a deep-sourced hydrothermal fluid containing sulfate approximating the lighter end-member moved upward and mixed with connate basin brines containing heavier sulfate. In this case the data could be recording progressive dilution of the hydrothermal fluid with basin waters as it moved upward through the section.

Whether or not mixing of fluids was an important factor in the deposition of the Northern Plomosa district barites, there is more than one possibility as to the mechanism of barite precipitation. Simple cooling of a barium- and sulfate-bearing hydrothermal solution as it migrated upward and mixed with lower temperature basin waters could have caused barite precipitation. Holland and Malinin (1979) indicate that in saline fluids barite solubility decreases

rapidly on cooling from 300 to 100°C.

Barium solubility in hydrothermal fluids, however, is in general quite low (Holland and Malinin, 1979), and therefore the large volume of barite mineralization in the area argues against a simple cooling model for precipitation. The strong association of barite mineralization with the upper, K-metasomatized part of the Tertiary section (Tv and Tpc) suggests that something unique to those rocks was important to barite precipitation. If the K-metasomatized rocks were enriched with barium, as indicated by Figure 12, then a sulfate-rich hydrothermal fluid coming into contact with those rocks would possibly be induced to precipitate barite. This scenario does not explain the observed mixing trend between heavy and light sulfate.

Relying on the inferred similarity between the mineralizing fluids and the presumably barium enriched K-metasomatizing fluids, still another possibility is suggested. Barium-rich hydrothermal fluids could have moved upward through the Tertiary section and precipitated barite upon mixing with sulfate-bearing basin waters. Stratification of both the composition and the amount of sulfate in the basin waters could account for the distribution of barite isotopic character and abundance observed in the stratigraphic column.

Carbonates

The carbonate rocks analyzed for carbon and oxygen isotopic composition include two different Tertiary limestones (red from the lower part and gray from the upper part of the T1st unit), a sample of Permian Kaibab limestone from the south side of Round mountain, and a carbonate lens from within the tectonized crystalline basement in the northwest corner of section 19. Hydrothermal carbonates analyzed include one malachite sample from the Heart's Desire mine in section 13, and five calcite samples from across the district.

Crushed calcite was reacted for two hours with 100% phosphoric acid at room temperature. The carbon dioxide gas produced by the reaction was processed in a high vacuum to remove any contaminants. The CO₂ was then analyzed for $\delta^{18}\text{O}$ and $\delta^{13}\text{C}$ on a VG602C double collector mass spectrometer in the Stable Isotope Laboratory at the University of Arizona. The data are precise to within 0.5‰ 2σ for both $\delta^{18}\text{O}$ and $\delta^{13}\text{C}$. Results are reported relative to standard mean ocean water (SMOW) for $\delta^{18}\text{O}$ and to PDB for $\delta^{13}\text{C}$. Dolomite and samples suspected to contain dolomite were treated in the same way except that they were reacted for 24 hours. The $\delta^{18}\text{O}$ result for the malachite sample was calculated as for dolomite.

Figure 27 is a plot of $\delta^{13}\text{C}$ against $\delta^{18}\text{O}$ for all of the carbonate samples analyzed. The two marine limestones fall within normal ranges of $\delta^{13}\text{C}$ and $\delta^{18}\text{O}$ for Permian and

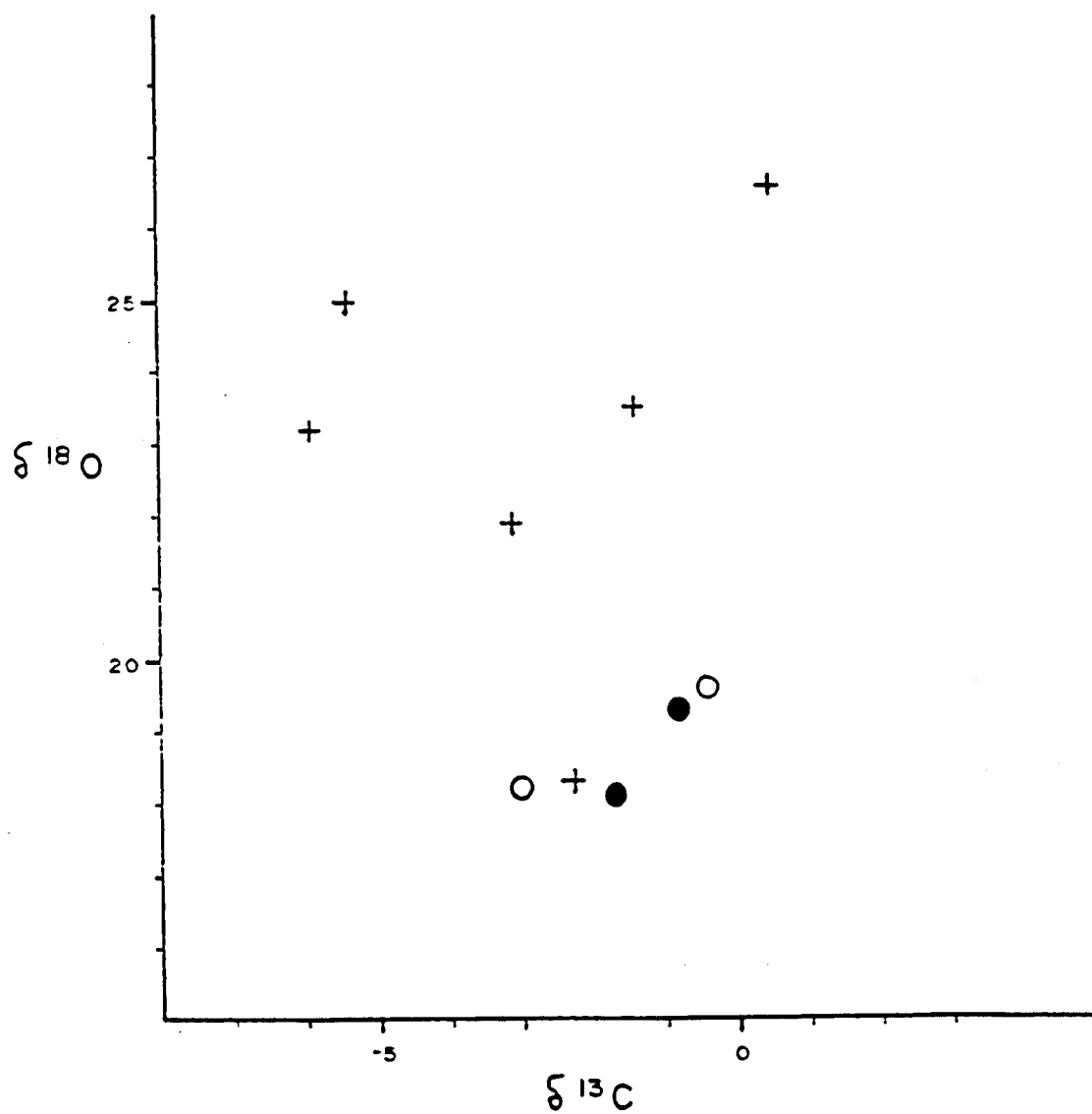


Figure 27- Plot of $\delta^{18}\text{O}$ vs. $\delta^{13}\text{C}$ values from carbonates in the Northern Plomosa district. Crosses represent hydrothermal minerals; filled circles represent Tertiary limestones, and open circles represent paleozoic carbonates.

Paleozoic/Proterozoic limestones as compiled by Veizer and Hoefs (1976). The Tertiary limestones are presumed to be non-marine in origin. Assuming a temperature of deposition of 25°C, they were deposited in equilibrium with water of -5 to -10‰ $\delta^{18}\text{O}$ range, using the curve produced by Friedman and O'Neil (1977, Figure 13). This is quite consistent with expected meteoric water values for the region in the Middle Tertiary (Field and Fifarek, 1985; Sheppard, 1986). No evidence of evaporitic enrichment is seen in the carbonate $\delta^{18}\text{O}$ values, but no significant difference in carbonate $\delta^{18}\text{O}$ values would be expected if these rocks had later equilibrated at low-temperature (75-100°C) with enriched K-metasomatizing brines of -2 to +4‰ $\delta^{18}\text{O}$.

The hydrothermal carbonates generally have higher $\delta^{18}\text{O}$ values than the sedimentary carbonates. No good control on temperature of deposition is available for the hydrothermal carbonates. Some are clearly hypogene, and probably deposited between 150 and 250°C, while others could be supergene. Even though no precise estimate of the $\delta^{18}\text{O}$ values of the waters can be made, all reasonable estimates indicate significantly higher values (+5 to +19‰ $\delta^{18}\text{O}$) than would be expected in normal meteoric water. The fluids were probably similar to the brines that deposited the barite and other minerals.

CHAPTER 8

Discussion and conclusions

The geologic history of the Northern Plomosa district is long and complex. It includes Proterozoic intrusion, deformation and possibly sedimentation, the deposition of Paleozoic and Mesozoic sedimentary and volcanic rocks and late Mesozoic folding and thrusting, followed by erosion to a deep level. The geological features of the Northern Plomosa district which are most important to this study, however, are all Tertiary in age. The event that began the transformation toward the present geological configuration was the initiation of large-magnitude extension and detachment faulting in the Early Miocene (Spencer et al., 1989).

The Tertiary sedimentary and volcanic section in the Northern Plomosa district is very similar to the many probably contemporaneous sedimentary and volcanic packages documented across the detachment faulted terrane of west-central Arizona and immediately adjacent California (Spencer and Reynolds, 1989b). These are interpreted to have been deposited in relatively small (short and long dimensions on the order of

5-10 and tens of km, respectively) closed basins immediately above or near the surface manifestations (break-aways) of the developing detachment faults (Figure 28) (Spencer, in press).

It seems likely that the break-away fault which was responsible for the formation of the basin into which the Tertiary sediments of the Northern Plomosa district were deposited was inactive, or nearly so, for some period after its initial development. The fine-grained clastic and carbonate sediments forming the T1st unit were probably deposited in a quiescent environment not affected by major faulting events. The interbedded tuffs in that unit, however, indicate that quiescence was not a regional phenomenon; explosive volcanism was occurring close enough to contribute volcanic ash to accumulating sediments. The thicker tuffs toward the top of the T1st unit and the relatively felsic compositions of the overlying volcanic unit in the eastern part of the study area suggest that the eruptive centers of felsic volcanic rocks were approaching the basin during the deposition of the T1st unit and were within the basin at the time of the eruption of agglomeratic members of the Tv unit. Felsite sills in the lower part of the Tertiary section could be comagmatic with the felsic tuffs of the T1st unit, and if so, would indicate that felsic volcanism was active within the basin before the end of the carbonate sedimentation.

The end of the relatively quiescent period in the

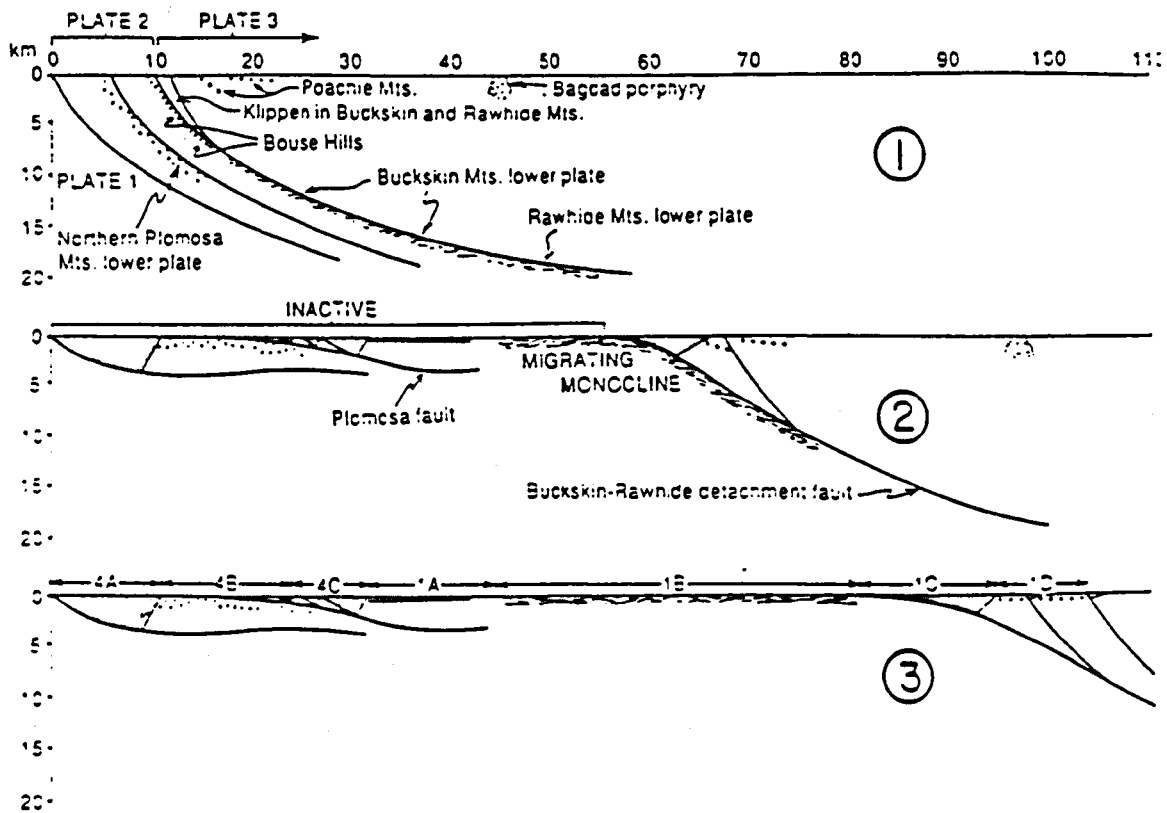


Figure 28- Cross-section of western Arizona showing the Plomosa detachment fault in its regional context, after Spencer and Reynolds (1990).

district is marked by the beginning of major local volcanism represented by the Tv unit. The presence of an angular unconformity between the T1st and Tv units that would indicate major tectonic activity preceding local volcanism was not noted in the course of this study. However, considering the poorly developed stratification in the volcanic unit and the common sheared or otherwise obscured contacts, evidence of an unconformity could easily have been missed. Scarborough and Meader (1982) did report minor angular unconformity (5-15 degrees) between the sedimentary and volcanic units on the basis of their regional mapping.

The flows, flow breccias, tuffs, and agglomerates of the volcanic unit constitute a significant thickness of volcanic material, much of it apparently quite proximal in source. No eruptive centers were identified, however, and no mafic dikes were observed to cut the underlying Tertiary sediments. A source outside the basin therefore seems likely.

Renewed faulting is suggested by the angular unconformity at the top of the volcanic unit and the very coarse and often angular nature of most of the overlying Plomosa conglomerate. Some earlier, probably fault-related relief is suggested by minor lenses of similar conglomerate within the volcanic unit, but by far the greatest volume of coarse clastic material is above the volcanic unit.

The fact that the Plomosa conglomerate is deposited only

on the volcanic unit, and that all identified clasts are pre-Tertiary, indicates that it was derived from a source outside of the basin, but deposited on top of a still basically undisturbed Tertiary section.

Field and geochemical evidence indicates (Chapter 3) that most of the Tertiary volcanic rocks in the Northern Plomosa district have been affected by potassium metasomatism. No evidence of K-metasomatism was found, however, in the mafic dikes within the Proterozoic sedimentary basement to the Tertiary section. Also, the basal Tertiary Bouse arkose is most commonly gray to gray-green in color and shows no sign of the pervasive oxidation which is a reliable indicator of K-metasomatism. No strong evidence was noted as to the degree to which the T1st unit might have been affected by metasomatizing fluids.

These observations indicate that the K-metasomatism was restricted to the higher levels of the basin stratigraphy. The cause of the evident confinement to higher levels is unknown, but geochemical or hydrologic stratification within the waters of the basin stratigraphy, such as that proposed in the discussion of stable isotope data, is suggested. It is reasonable to suspect that the laminated carbonates, silts, and tuffs of the T1st unit could have formed an effective aquiclude, blocking the metasomatizing effects of the higher level brines. This inference would also imply that at the

time of K-metasomatism the Tertiary sedimentary section was still largely intact and unaffected by listric faulting and block rotation. In any case, pervasive K-metasomatism by deep-level waters is not indicated.

The escape from complete K-metasomatism of at least one basaltic flow within the Tertiary Volcanic unit (sample #11-28-12) is difficult to explain. This particular sample is a dense, non-vesicular, non-brecciated rock in close proximity to a Plomosa conglomerate lens. A large difference in permeability between the two lithologies might have channeled metasomatizing fluids through the conglomerate in preference to the basalt, resulting in a lower water-rock ratio and relatively little alteration in that instance.

Roddy et al. (1988) found that K-metasomatism preceded detachment-related mineralization, and inferred that basinal brines acting at low temperatures (80-120°C) were responsible. No evidence was found in this investigation to contradict these findings. The observations just cited tend to support the interpretation that the fluids responsible were shallow in source, and that there was a definite floor to their effects. The interpretation that K-metasomatism preceded mineralization is supported by the fact that mineralization and related alteration affect all of the Tertiary section and the Proterozoic sedimentary basement, and are concentrated along listric normal faults which must have developed after

K-metasomatism.

Evidence that the hydrothermal mineralization occurred quite late in the development of the present geologic configuration includes the fact that amethyst-hematite veins cut the Plomosa conglomerate on Beehive hill. The amethyst veins are thought to represent the earliest stage of Tertiary mineralization in the district (see Chapter 4), and yet they form well-defined veins in the conglomerate, indicating that it was already well-indurated by the time of the earliest hydrothermal activity. This would place the time of mineralization significantly later than the latest known igneous activity in the area.

The paragenetic and fluid-inclusion data indicate that most of the mineralization in the Northern Plomosa district is part of one integrated system that developed late in the evolution of the detachment-fault terrane as now exposed. Minor postdetachment mineralization is later than the main event, and distinct in its mineralogy and chemistry. It seems likely that the main mineralization occurred contemporaneously with detachment faulting because of its concentration in northwest-striking detachment-related listric normal faults that would have been active and dilatant during the regional extensional event. The brecciated nature of some of the vein mineralization is probably due to synchronous fault movement and mineralization. The lack of significant mineralization

or alteration in the Plomosa detachment fault or in the immediately adjacent lower plate suggests that detachment fault movement continued beyond the time of mineralization, placing altered and mineralized upper plate rocks against unaltered lower plate rocks.

The timing of mineralization and association with detachment-related structures, the proximity of the Plomosa detachment fault, and the strong similarity of local mineralization (see Chapters 4 and 5) to recognized detachment-related mineralization in the region (Spencer and Welty, 1989; Wilkins, et al., 1986) all lead to the classification of the district as a part of that group.

The high inferred salinities and oxidized nature of the fluids involved in the Northern Plomosa hydrothermal system suggest that the metals might have been transported as chloride complexes. Under low-temperature conditions such as those which prevailed in the Northern Plomosa system, chloride complexing is generally considered secondary to bisulfide complexing in importance in mobilizing metals (reference). However, both Kuen (1988) and Wilkins et al. (1986) have shown that under highly saline and oxidizing conditions chloride complexing can be important at low to moderate temperatures (>200°C). The late nature of the gold in the Northern Plomosa district combined with the homogenization temperature increases in the latest, still high-salinity fluid inclusions

suggests that significant gold transport took place only when, during late-stage rejuvenation, the hydrothermal system reached the high salinity, higher temperature conditions that promoted chloride-complex stability.

REFERENCES CITED

- Allen, G.B., 1985, Economic geology of the Bighorn Mountains of west-central Arizona: Arizona Bureau of Geology and Mineral Technology Open-File Report 85-17, 140 p.
- Bancroft, Howland, 1911, Reconnaissance of the ore deposits in northern Yuma County, Arizona: U.S. Geological Survey Bulletin 451, 130p.
- Beane, R.E., Wilkins, Joe, Jr., and Heidrick, T.L., 1986, A geochemical model for gold mineralization in the detachment fault environment, *in* Beatty, Barbara, and Wilkinson, P.A.K., eds., *Frontiers in geology and ore deposits of Arizona and the Southwest*: Arizona Geological Society Digest, v. 16, p. 222.
- Bean, Richard, Wilkins, Joe, Jr., and Heidrick, Tom, 1988, Conditions of gold mineralization in the detachment fault environment, *in* Dummett, Hugo, and Colburn, Nora, eds., *Field Trip to Bighorn Mine, Socorro Mine, and Copperstone Mine, Arizona; Arizona Geological Society Spring Field Trip, 1988*: Arizona Geological Society, 1988.
- Bradley, M.A., 1987, Vein mineralogy, paragenetic sequence and fluid inclusion survey of the Silver District, La Paz Co., Arizona: Tucson, University of Arizona, unpublished Masters thesis, 131 p.
- Brooks, W.E., 1985, Analyses of upper-plate volcanic rocks at Picacho Peak, Pinal County, Arizona: U.S. Geological Survey Open-File Report 85-740, 5 p.
- _____ 1986, Distribution of anomalously high K_2O volcanic rocks in Arizona: *Metasomatism at the Picacho Peak detachment fault*: *Geology*, v. 14, p. 339-342.
- _____ 1988, Recognition and geologic implications of Potassium metasomatism in upper-plate at the detachment fault at the Harcuvar Mountains, Yavapai County, Arizona: U.S. Geological Survey Open-File Report 88-17, 9 p.

- Bryant, B., and Wooden, J.L., 1989, Lower-plate rocks of the Buckskin Mountains, Arizona: a progress report, in Spencer, Jon E., and Reynolds, Stephen J., eds., Geology and mineral resources of the Buckskin and Rawhide Mountains, west-central Arizona: Arizona Geological Survey Bulletin 198, p. 47-50.
- Chapin, C.E., and Lindley, J.I., 1986, Potassium metasomatism of igneous and sedimentary rocks in detachment terranes and other sedimentary basins: Economic implications, in Beatty, Barbara, and Wilkinson, P.A.K., eds., Frontiers in geology and ore deposits of Arizona and the Southwest: Arizona Geological Society Digest, v. 16, p. 118-126.
- Chiba, Hitoshi, and Sakai, Hitoshi, 1985, Oxygen isotope exchange rate between dissolved sulfate and water at hydrothermal temperatures: *Geochemica et Cosmochemica Acta*, v. 49, p. 993-1000.
- Claypoole, G.E., Holser, W.T., Kaplan, I.R., Sakai, Hitoshi, and Zak, Israel, 1980, The age curves of sulfur and oxygen isotopes in marine sulfate and their mutual interpretation: *Chemical Geology*, v. 28, p.199-260.
- Coney, P.J., 1974, Structural analysis of the Snake Range "decollement," east-central Nevada: *Geological Society of America Bulletin*, v. 85, p. 973-978.
- _____, 1980, Cordilleran Metamorphic core complexes: An overview: in Crittenden, M.D., Jr., and others, eds., Cordilleran metamorphic core complexes: Geological Society of America Memoir 153, p. 7-31.
- Crawford, M.L., Krouse, D.W., and Hollister, L.S., 1979, Petrologic and fluid inclusion study of calc-silicate rocks, Prince Rupert, British Columbia: *American Journal of Science*, v. 279, p. 1135-1159.
- Davis, G.A., 1989, Terry Shackelford and the Rawhide Mountains: a retrospective view, in Spencer, Jon E., and Reynolds, Stephen J., eds., Geology and mineral resources of the Buckskin and Rawhide Mountains, west-central Arizona: Arizona Geological Survey Bulletin 198, p. 47-50.
- Davis, G.H., 1983, Shear-zone model for the origin of metamorphic core complexes: *Geology*, v. 7, p. 120-124.

- Davis, J.C., 1986, *Statistics and Data Analysis in Geology*, Second Edition, John Wiley and Sons, Inc., New York, 646 p.
- Field, C.W., and Fifarek, R.H., 1985, Light stable-isotope systematics in the epithermal environment, *in* Berger, B.R., and Bethke, P.M., eds., *Geology and geochemistry of epithermal systems: Reviews in Economic Geology*, v. 2, p. 99-128.
- Friedman, I., and O'Neil, J.R., 1977, Compilation of stable isotope fractionation factors of geochemical interest, *in* Fleischer, M., ed., *Data of geochemistry*, sixth edition: U.S. Geological Survey Professional Paper 440-KK, p. KK1-KK12.
- Grant, J.A., 1986, The isocon diagram- a simple solution to Gresen's equation for metasomatic alteration: *Economic Geology*, v. 81, p. 1976-1982.
- Holland, H.D., and Malinin, S.D., 1979, The solubility and occurrence of non-ore minerals, *in* Barnes, H.L., ed., *Geochemistry of Hydrothermal Ore Deposits*, Second Edition: John Wiley and Sons, New York, p. 461-508.
- Jemmett, J.P., 1966, *Geology of the Northern Plomosa Mountain Range, Yuma County, Arizona*: Tucson, University of Arizona, unpublished Ph.D. dissertation, 128 p.
- Keith, Stanley B., Gest, D.E., DeWitt, Ed, Woode Toll, Netta, and Everson, B.A., 1983, *Metallic mineral districts and production in Arizona*: Arizona Bureau of Geology and Mineral Technology Bulletin 194, 58 p.
- Kerrich, R., Rehrig, W.A., and McLarty, E., 1989, Volcanic rocks in the suprastructure of metamorphic core complexes, southwest Arizona: geochemical and isotopic evidence for primary magma types and secondary magma regimes, *in* Spencer, Jon E., and Reynolds, Stephen J., eds., *Geology and mineral resources of the Buckskin and Rawhide Mountains, west-central Arizona*: Arizona Geological Survey Bulletin 198, p. 203-214.
- Kuehn, K.A., 1988, A general comment on FeOx-gold deposits and gold solubility, *in* Dummett, Hugo, and Colburn, Nora, eds., *Field Trip to Bighorn Mine, Socorro Mine, and Copperstone Mine, Arizona*; Arizona Geological Society Spring Field Trip, 1988: Arizona Geological Society, 1988.

- Laskey, S.G., and Webber, B.N., 1949, Manganese resources of the Artillery Mountains region, Mohave County, Arizona: U.S. Geological Survey Bulletin 961, 86 p.
- Lucchita, Ivo, and Suneson, Neil, 1981, Comment on Tertiary tectonic denudation of a Mesozoic-early Tertiary(?) gneiss complex, Rawhide Mountains, western Arizona: *Geology*, V. 9, p. 50-51.
- Newell, R.A., 1974, Exploration geology and geochemistry of the Tombstone-Charleston area, Cochise County, Arizona: unpublished Ph.D dissertation, Stanford University.
- Potter, R.W., II, 1977, Pressure corrections for fluid inclusion homogenization temperatures based on volumetric properties for the system NaCl-h₂o: U.S. Geological Survey Journal of Research, v. 5, p. 603-607.
- Reynolds, S.J., and Spencer, J.E., 1985, Evidence for large-scale transport on the Bullard detachment fault, west-central Arizona: *Geology*, v.13, p. 353-356.
- Reynolds, S.J., 1988, Geologic map of Arizona: Arizona Geological Survey Map 26.
- Reynolds, S.J., Spencer, J.E., Richard, S.M., and Laubach, S.E., 1986, Mesozoic structures in west-central Arizona, in Beatty, Barbara, and Wilkinson, P.A.K., eds., *Frontiers in geology and ore deposits of Arizona and the Southwest: Arizona Geological Society Digest*, v. 16, p. 35-51.
- Roddy, M.S., Reynolds, S.J., Smith, B.M., and Ruiz, Joaquin, 1988, K-metasomatism and detachment-related mineralization, Harcuvar Mountains, Arizona: *Geological Society of America Bulletin*, v. 100, p. 1627-1639.
- Scarborough, Robert, and Meader, Norman, 1982, Reconnaissance geology of the northern Plomosa Mountains, Arizona: Arizona Bureau of Geology and Mineral Technology Open-File Report 83-24, 35 p.
- _____, 1989, Geologic map of the Northern Plomosa Mountains, Yuma County, Arizona: Arizona Geological Survey Contributed Map 89D.

- Shackelford, T.J., 1976, Structural geology of the Rawhide Mountains, Mojave County, Arizona: Los Angeles, University of Southern California, unpublished Ph.D. dissertation, 176 p.
- _____, 1989, Structural geology of the Rawhide Mountains, Mohave County, Arizona, *in* Spencer, Jon E., and Reynolds, Stephen J., eds., Geology and mineral resources of the Buckskin and Rawhide Mountains, west-central Arizona: Arizona Geological Survey Bulletin 198, p. 15-46.
- Spencer, J.E., 1984, Geometry of low-angle normal faults in west-central Arizona: Arizona Bureau of Geology and Mineral Technology Fieldnotes, v. 14, no. 3, p. 6-8.
- Spencer, J.E., Duncan, J.T., and Burton, W.D., 1988, The Copperstone mine: Arizona's new gold producer: Arizona Bureau of Geology and Mineral Technology Fieldnotes, v. 18, no. 2, p.1-3.
- Spencer, J.E., and Reynolds, S.J., 1989a, Introduction to the geology and mineral resources of the Buckskin and Rawhide Mountains, *in* Spencer, Jon E., and Reynolds, Stephen J., eds., Geology and mineral resources of the Buckskin and Rawhide Mountains, west-central Arizona: Arizona Geological Survey Bulletin 198, p. 1-10.
- _____, 1989b, Tertiary structure, stratigraphy and tectonics of the Buckskin Mountains, *in* Spencer, Jon E., and Reynolds, Stephen J., eds., Geology and mineral resources of the Buckskin and Rawhide Mountains, west-central Arizona: Arizona Geological Survey Bulletin 198, p. 103-167.
- _____, 1990, Tectonics of mid-Tertiary extension along a transect through west-central Arizona, submitted to Geological Society of America Bulletin (in review 6-90), 39p.
- Spencer, J.E., Shaffiqulla, M., Miller, R.J., and Pickthorn, L.G., 1989 K-Ar geochronology of miocene extension, volcanism, and potassium metasomatism in the Buckskin and Rawhide Mountains, *in* Spencer, Jon E., and Reynolds, Stephen J., eds., Geology and mineral resources of the Buckskin and Rawhide Mountains, west-central Arizona: Arizona Geological Survey Bulletin 198, p. 184-189.

- Spencer, J.E., and Welty, J.W., 1985, Reconnaissance geology of mineralized areas in parts of the Buckskin, Rawhide, McCracken, and northeastern Harcuvar mountains, western Arizona: Arizona Bureau of Geology and Mineral Technology Open-File Report 85-6, 31 p.
- _____. 1986, Possible controls of base- and precious-metal mineralization associated with Tertiary detachment faults in the lower Colorado River trough, Arizona and California: *Geology*, v. 14. p. 195-198.
- _____. 1989, Geology of mineral deposits in the Buckskin and Rawhide Mountains, *in* Spencer, Jon E., and Reynolds, Stephen J., eds., *Geology and mineral resources of the Buckskin and Rawhide Mountains, west-central Arizona*: Arizona Geological Survey Bulletin 198, p. 223-254.
- Stone, Claudia, 1989, A summary appraisal of the principal geothermal resource areas in arizona, *in* Jenney, J.P., and Reynolds, S.J., 1989, *Geologic evolution of Arizona*: Tucson, Arizona Geological Society Digest 17, p.817-825.
- Veizer, J., and Hoefs, J., 1976, The nature of O^{18}/O^{16} and C^{13}/C^{12} secular trends in sedimentary carbonate rocks: *Geochemica et Cosmochemica Acta*, v. 40, p. 1387-1395.
- Wernicke, Brian, 1981, Low-angle normal faults in the Basin and Range Province: Nappe tectonics in an extending orogen: *Nature*, v. 291, p. 645-648.
- Wilkins, Joe, Jr., Beane, R.E., and Heidrick, T.L., 1986, Mineralization related to detachment faults: A model, *in* Beatty, Barbara, and Wilkinson, P.A.K., eds., *Frontiers in geology and ore deposits of Arizona and the Southwest*: Arizona Geological Society Digest, v. 16, p. 108-117.
- Wilkins, Joe, Jr., and Heidrick, T.L., 1982, Base and precious metal mineralization related to low angle tectonic features in the Whipple Mountains, California and Buckskin Mountains, Arizona, *in* Frost, E.G., and Martin, D.L., eds., *Mesozoic-Cenozoic tectonic evolution of the Colorado River region, California, Arizona, and Nevada*: San Diego, Cordilleran Publishers, p. 128-203.
- Wilson, E.D., 1960, Geologic map of Yuma County, Arizona: Arizona Bureau of Mines, scale 1:375,000.

Faint, illegible text at the top of the page, possibly a header or title.

Second block of faint, illegible text.

Third block of faint, illegible text.

5
25/1/19
1/10

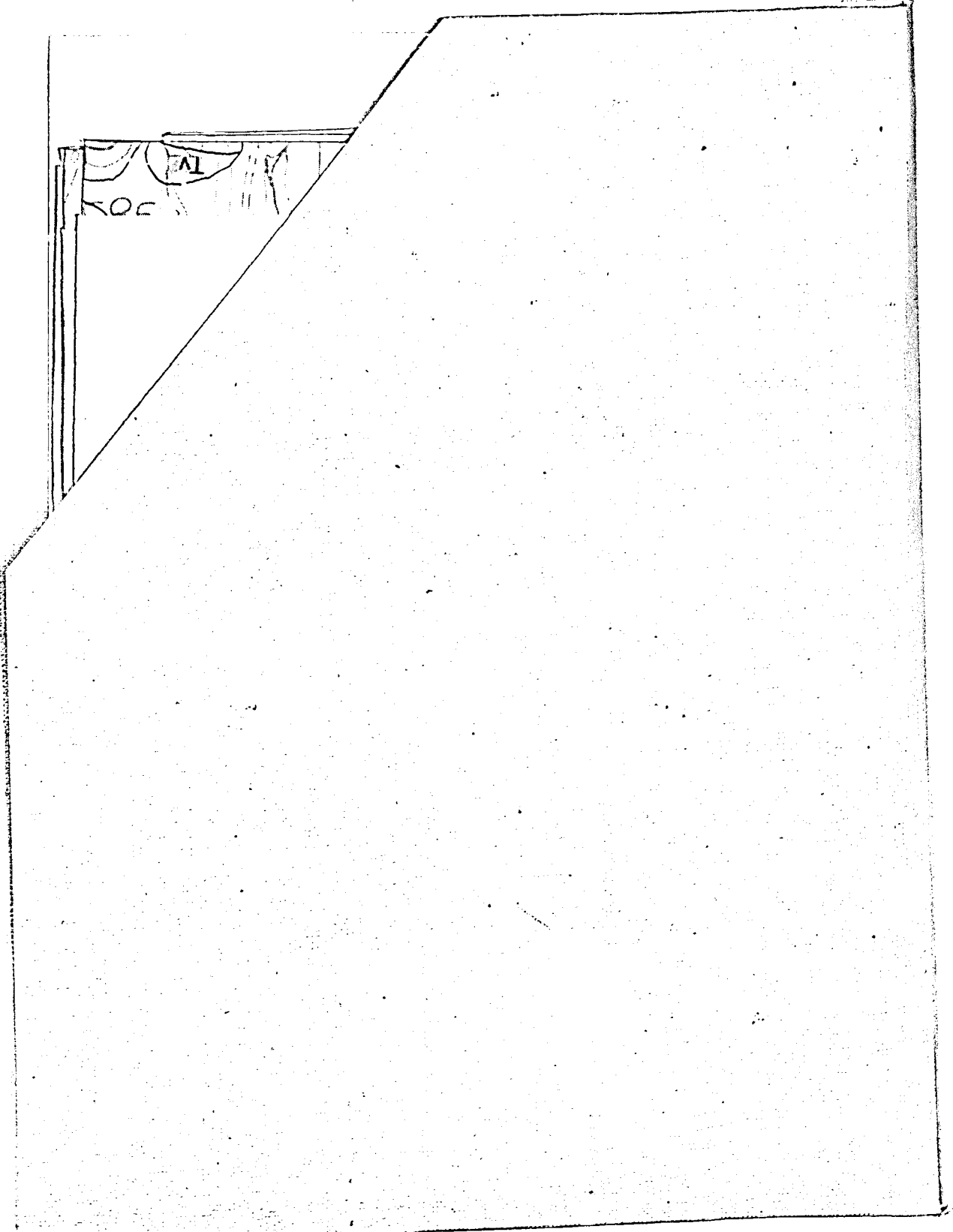




PLATE I

GEOLOGIC MAP
OF
THE NORTHERN PLOMOSA DISTRICT,
LA PAZ COUNTY, ARIZONA

LEGEND:

Quaternary

Qs Quaternary surficial deposits

Tertiary

- Tif Fine-grained felsic intrusions
- Tim Fine-grained mafic intrusions
- Tpc Plomosa Conglomerate
- Tv Volcanic unit
- Tlst Limestone-tuff unit (Tls = Limestone)
- Tba Bouse Arkose

Mesozoic & Paleozoic

- Tb Triassic Buckskin Formation
- Pk Permian Kaibab Formation
- Ps Pennsylvanian Supai Group
- MDC Mississippian to Devonian Martin/Redwall Formations
- Ca Cambrian Abrigo Formation
- Cb Cambrian Bolsa Quartzite
- PZc Undifferentiated Paleozoic carbonate rocks
- PZq Undifferentiated Paleozoic quartzite

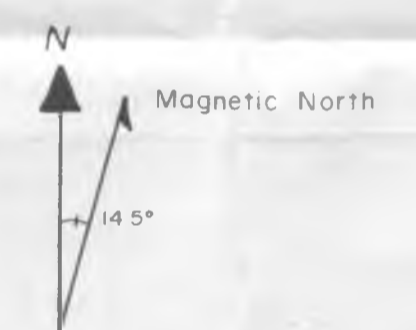
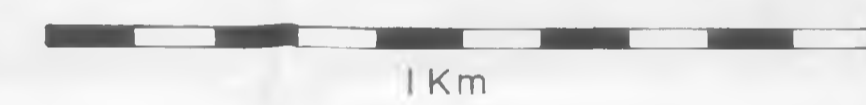
Precambrian

pCg Precambrian granitic to gneissic/mylonitic crystalline rocks

Lower Plate

lpm Undifferentiated lower plate metamorphic rocks

- contact (dashed where approx. located)
- - - - - fault (dashed where inferred; dotted where covered.) arrow indicates dip
- - - - - detachment fault
- - - - - low angle (<30°) normal fault
- - - - - thrust fault
- 40 dip & strike of carbonate beds or slivers in mylonitic Precambrian crystalline rock
- 20 trend & plunge of mylonitic lineation in pC basement

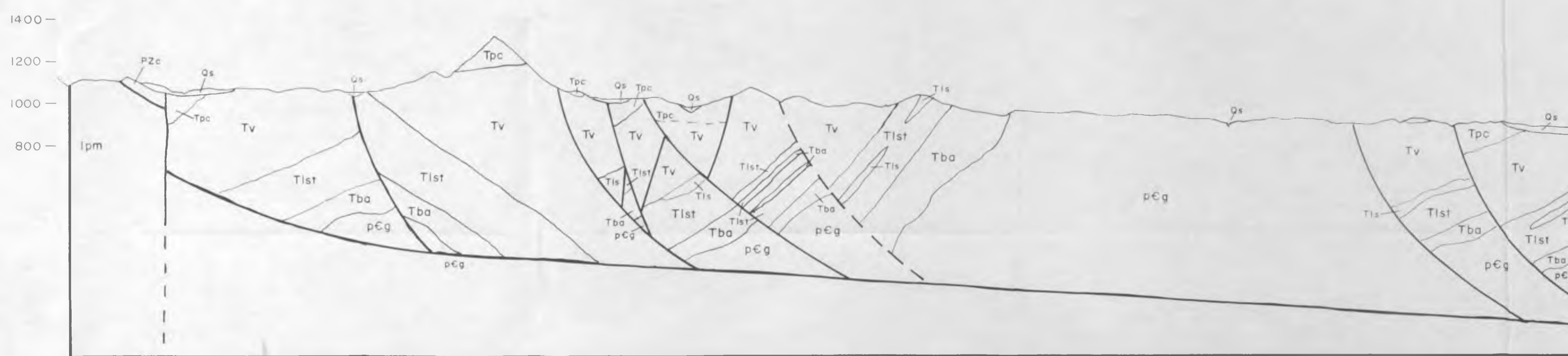


by:

JOHN TOWNER DUNCAN

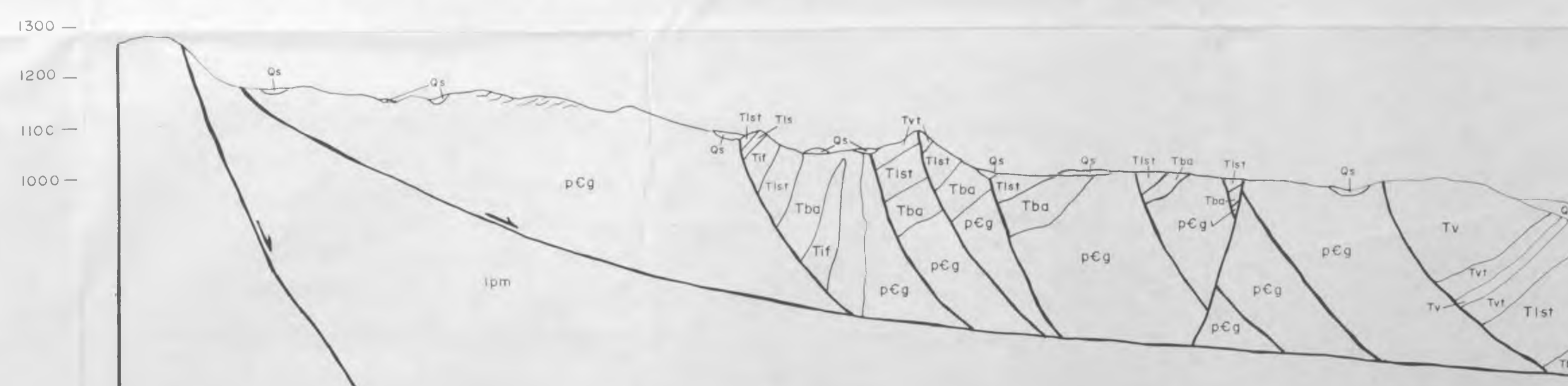
Round Mtn Thrust block (SE 1/4 S.19)
mapped by Stephen J. Reynolds

A-A'



Vertical exaggeration
approximately 2X.

B-B'



Vertical exaggeration
approximately 4X.

JOHN TOWNER DUNCAN
UNIVERSITY OF ARIZONA
DEPARTMENT OF GEOSCIENCES
M.S. THESIS 1990

E 9791

1990

304

~~1990~~

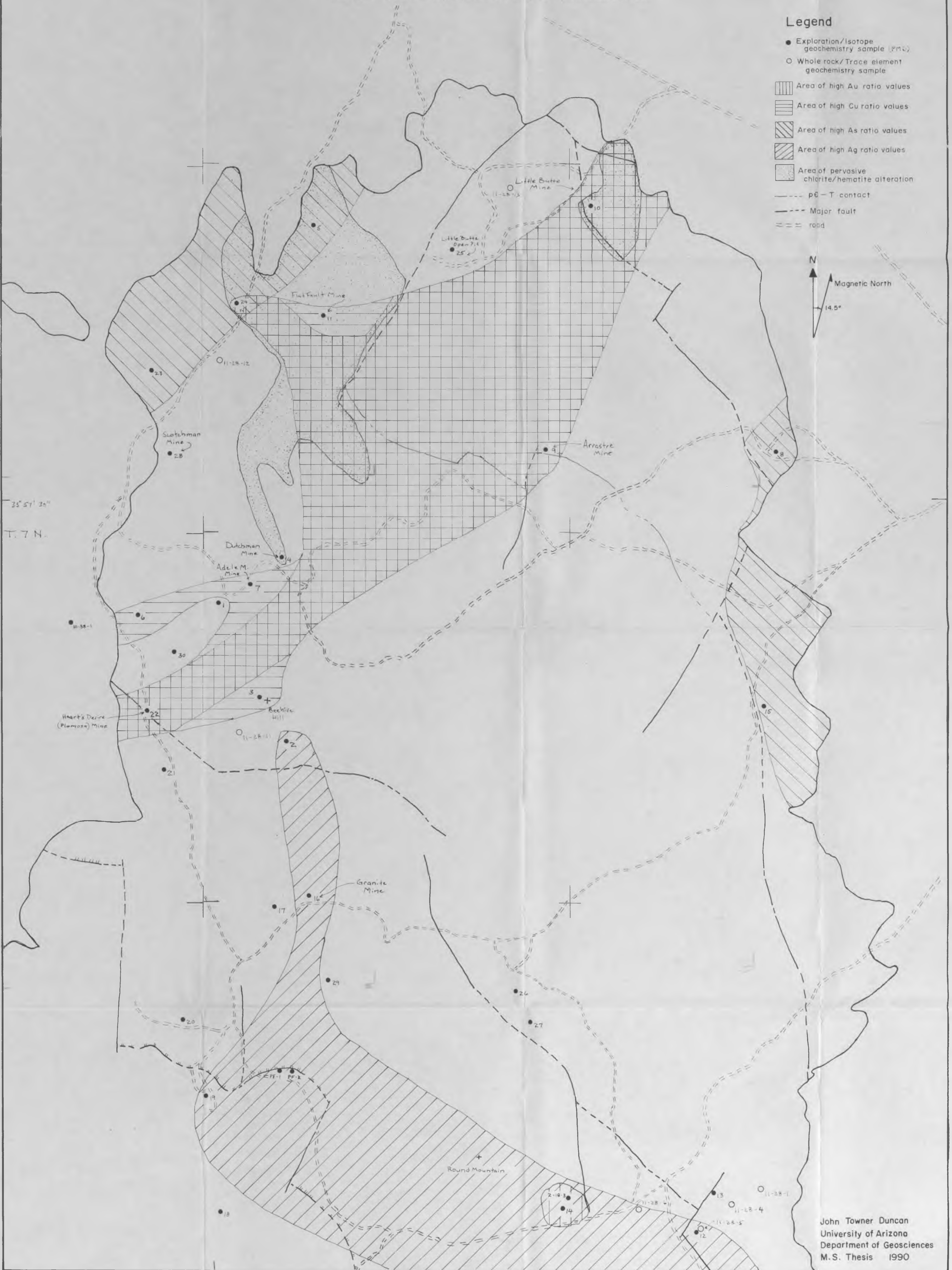
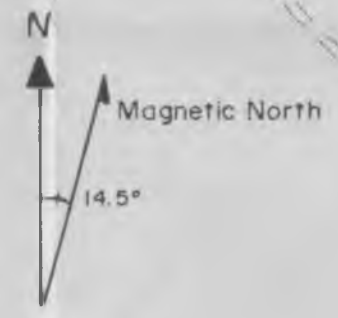
1

NORTHERN PLOMOSA DISTRICT

Sample Locations, Geochemistry & Mineralization

Legend

- Exploration/Isotope geochemistry sample (P.M.U.)
- Whole rock/Trace element geochemistry sample
- ▨ Area of high Au ratio values
- ▧ Area of high Cu ratio values
- ▩ Area of high As ratio values
- Area of high Ag ratio values
- ▤ Area of pervasive chlorite/hematite alteration
- - - pE-T contact
- - - Major fault
- == road



John Towner Duncan
University of Arizona
Department of Geosciences
M.S. Thesis 1990

E9791

1990

304

Spec. City